Cell-type specific circadian bioluminescence rhythms recorded from *Dbp* reporter mice reveal circadian oscillator misalignment

[a,b,1] Ciearra B. Smith, [a,c,1] Vincent van der Vinne, [d] Eleanor McCartney, [e] Adam C. Stowie, [f] Tanya L. Leise, [d,2] Blanca Martin-Burgos, [d] Penny C. Molyneux, [g] Lauren A. Garbutt, [h] Michael H. Brodsky, [e] Alec J. Davidson, [d] Mary E. Harrington, [g] Robert Dallmann, and [a,b,j,3] David R. Weaver

[a] Department of Neurobiology, University of Massachusetts Medical School, Worcester MA

[b] Graduate Program in Neuroscience, University of Massachusetts Medical School, Worcester MA

[c] Department of Biology, Williams College, Williamstown, MA

[d] Neuroscience Program, Smith College, Northampton MA

[e] Neuroscience Institute, Morehouse School of Medicine, Atlanta GA

[f] Department of Mathematics and Statistics, Amherst College, Amherst MA

[g] Division of Biomedical Sciences, Warwick Medical School, University of Warwick, Coventry, UK

[h] Department of Molecular, Cell and Cancer Biology, University of Massachusetts Medical School, Worcester MA

[i] Department of Biochemistry and Molecular Pharmacology, University of Massachusetts Medical School, Worcester MA

[j] NeuroNexus Institute, University of Massachusetts Medical School, Worcester MA

[1] C.B.S and V.v.d.V contributed equally to this work.

[2] Present address: University of California, San Diego, La Jolla, CA USA

[3] To whom correspondence may be addressed:

Email: David.weaver@umassmed.edu

David R. Weaver, Ph.D., Department of Neurobiology, LRB-723, UMass Medical School, 364 Plantation St., Worcester MA 01605

ORCID ID's:

CBS	0000-0003-2999-3387	Ciearra.Smith@umassmed.edu
VvdV	0000-0003-3926-5041	vv5@williams.edu
EM	0000-0002-5806-1995	mccartneyee1921@gmail.com
ACS	0000-0002-7007-9135	astowie@msm.edu
TLL	0000-0002-7458-7604	tleise@amherst.edu
BMB	0000-0002-1388-9123	bmartinb@ucsd.edu
PCM		pmolyneu@smith.edu
LAG	0000-0002-9366-4468	L.A.Garbutt@warwick.ac.uk
MHB	0000-0001-7703-4872	Michael.brodsky@umassmed.edu
AJD	0000-0003-4205-1968	adavidson@msm.edu
MEH	0000-0003-2266-6455	mharring@smith.edu
RD	0000-0002-7490-0218	R.Dallmann@warwick.ac.uk
DRW	0000-0001-7941-6719	david.weaver@umassmed.edu

Classification

Major Classification: Biological Sciences

SubClassification: Physiology

Keywords (at least three and no more than five).

Circadian Rhythms, Bioluminescence, Luciferase, Misalignment, Liver

Conflict of interest statement: The authors declare no conflicts of interest.

This PDF contains

Main Text

Figures 1 to 7

Table 1

Abstract

Circadian rhythms are endogenously generated physiological and molecular rhythms with a cycle length of about 24 h. Bioluminescent reporters have been exceptionally useful for studying circadian rhythms in numerous species. Here, we report development of a reporter mouse generated by modification of a widely expressed and highly rhythmic gene encoding D-site albumin promoter binding protein (*Dbp*). In this line of mice, firefly luciferase is expressed from the *Dbp* locus in a *Cre*-recombinase-dependent manner, allowing assessment of bioluminescence rhythms in specific cellular populations. A mouse line in which luciferase expression was *Cre*-independent was also generated. The *Dbp* reporter alleles do not alter *Dbp* gene expression rhythms in liver or circadian locomotor activity rhythms. *In vitro* and *in vivo* studies show the utility of the reporter alleles for monitoring rhythmicity. Our studies reveal cell-type specific characteristics of rhythms among neuronal populations within the suprachiasmatic nuclei *in vitro*. *In vivo* studies show stable *Dbp*-driven bioluminescence rhythms in the liver of *Albumin-Cre;Dbp*$^{KI/+}$ "liver reporter" mice. After a shift of the lighting schedule, locomotor activity achieved the proper phase relationship with the new lighting cycle more rapidly than hepatic bioluminescence did. As previously shown, restricting food access to the daytime altered the phase of hepatic rhythmicity. Our model allowed assessment of the rate of recovery from misalignment once animals were provided with food *ad libitum*. These studies provide clear evidence for circadian misalignment following environmental perturbations and reveal the utility of this model for minimally invasive, longitudinal monitoring of rhythmicity from specific mouse tissues.

76 ***Significance Statement***

77 Disruption of temporal coordination among circadian oscillators and exposure to light at
78 biologically inappropriate times are important drivers of the increased incidence of adverse health
79 outcomes observed in shift workers and rodent models of chronic circadian disruption. Here, we
80 demonstrate the utility of a new mouse line that enables tissue-specific monitoring of circadian
81 molecular rhythms *in vivo* and *ex vivo*. This reporter mouse provides a major advance in our
82 capabilities for monitoring rhythms in a variety of tissues under normal and disruptive conditions.
83 Our studies provide an unprecedented longitudinal assessment of tissue-specific rhythmicity, a key
84 step in the identification of mechanisms underlying the circadian disruption inherent to life in
85 modern 24/7 societies.

86

87 **Introduction**

88 Circadian rhythms are endogenous rhythms with a cycle length of ~24 hours. The mammalian
89 circadian system is hierarchical. The hypothalamic suprachiasmatic nuclei (SCN) serve as the pacemaker[1,2].
90 The SCN are synchronized by environmental cues, of which the light-dark cycle is the most influential. The
91 SCN are not unique in their capacity for rhythmicity, however. The transcriptional-translational feedback
92 loop regulating molecular oscillations in the SCN is also present in individual cells throughout the body[1,2].
93 SCN-driven neural, behavioral and hormonal rhythms synchronize these cell-autonomous oscillators,
94 leading to rhythmicity with predictable phase relationships among tissues, genes and physiological
95 processes[1-4]. Repeated disruption of this internal temporal order by inappropriately timed light exposure or
96 food intake leads to adverse health consequences in shift-working humans and animal models[4-15]. Progress
97 in identifying the mechanisms by which chronic circadian disruption leads to adverse health consequences
98 will require long-term monitoring of central and peripheral rhythms[7,8].

99 Rhythmically expressed reporter genes have been extremely important for demonstrating cell-
100 autonomous circadian clocks in several organisms[16-23], and in screens identifying clock genes and
101 modifiers[24-28]. Circadian reporters have also been used to assess rhythmicity in peripheral tissues and the
102 impact of dynamic alterations in environmental conditions (food availability, lighting cycles) on peripheral
103 oscillators, conducted by measuring bioluminescence rhythms in tissue explants monitored *ex vivo*[21,29-35].
104 These studies complement work done by assessing population rhythms in gene expression in tissue
105 samples[36-42] indicating altered rhythm amplitude, phase, and phase relationships in and between SCN and
106 peripheral oscillators following resetting[43]. More recent advances include development of methods for
107 monitoring bioluminescence rhythms from the SCN *in vivo*[44-50], and for assessing peripheral rhythms in
108 anesthetized[51-53] and ambulatory[54,55] mice.

109 Here, we report a new transgenic mouse line in which firefly luciferase is expressed from the mouse
110 *Dbp* locus in a *Cre*-recombinase-dependent manner. *Dbp* is widely and rhythmically expressed[3,57], allowing
111 detection of circadian bioluminescence rhythms in numerous tissues, *in vivo* and *ex vivo*. *Cre*-dependent
112 bioluminescence in specific cell types revealed unexpected differences among SCN neuronal populations.

113 Furthermore, we observed transient misalignment between behavioral and hepatic bioluminescence
114 rhythms in freely moving mice subjected to a shift of the light-dark cycle or restricted food access.
115
116 **Results**
117 **Generation of a bifunctional reporter mouse.** CRISPR/Cas9 genome editing was used to introduce a
118 bifunctional reporter into the mouse *Dbp* locus (**Fig. 1**). The reporter consists of a T2A sequence (to allow
119 expression of separate proteins from a single transcript[56]), a destabilized, enhanced GFP (d2EGFP, hereafter
120 GFP) sequence flanked by loxP sites, and a codon optimised synthetic firefly *luciferase* (luc2 from
121 *Photinus pyralis,* hereafter luc). In the absence of *Cre* expression, DBP and GFP are expressed as separate
122 proteins. After CRE-mediated recombination, the floxed GFP is removed, and separate DBP and luciferase
123 proteins are expressed from the *Dbp* locus. Sequencing of genomic DNA confirmed successful generation
124 of the Dbp^{KI} conditional reporter allele.
125
126 **GFP expression from the Dbp^{KI} allele.** To examine expression of GFP from the conditional allele, $Dbp^{KI/+}$
127 mice (n=5-6 mice per time-point) were anesthetized and perfused with fixative at 4-h intervals over 24 h
128 (**Fig. S1**). Liver sections from $Dbp^{KI/+}$ and control (WT) mice were examined by confocal microscopy.
129 Fluorescence signal intensity did not differ between time-points (ANOVA $F_{5,26}$ =1.279, p = 0.7560). GFP
130 signal from $Dbp^{KI/+}$ liver sections was 5-10x higher than from WT sections, but absolute levels were quite
131 low. The low level of GFP expression may be due to the use of destabilized GFP with a 2-hour half-life,
132 intended to more accurately track changes on a circadian time-scale. The relatively low level and lack of
133 detectable rhythmicity in GFP expression was unexpected, especially considering that liver is the tissue
134 with the highest levels of *Dbp* expression[57] and thus may represent a 'best-case' scenario. As the primary
135 objective of this project was to generate a mouse model with Cre-dependent expression of bioluminescence
136 from the *Dbp* locus, however, the absence of robust GFP-driven fluorescence rhythms in *Cre*-negative cells
137 did not preclude achieving this objective. GFP is effectively serving as a 'floxed stop' to make luciferase
138 expression from the *Dbp* locus exclusively *Cre*-dependent.

139

140 **<u>Non-conditional luciferase expression from the *Dbp*^{Luc} allele.</u>** A non-conditional reporter allele was
141 generated by breeding to combine the conditional *Dbp*^{KI} allele with *Cre*-recombinase expressed in the
142 germline, leading to germline excision of GFP. The resulting *Dbp*^{Luc} allele produces wide-spread, rhythmic
143 luciferase expression, both and *in vivo* and *ex vivo*. More specifically, explants of lung and anterior pituitary
144 gland from *Dbp*$^{Luc/+}$ mice incubated with D-luciferin had robust circadian rhythms in bioluminescence (**Fig.**
145 **2**). Furthermore, *in vivo* imaging of *Dbp*$^{Luc/+}$ mice at 7 time-points over a ~30-h period revealed rhythmic
146 bioluminescence in the abdomen and throat in ventral views, and in the lower back in dorsal views (**Fig.**
147 **3B**), similar to the distribution of bioluminescence signal from *Per2*^{Luc} mice[51-53] (**Fig. 3A**). The level of
148 light output was ~2.5-fold greater in ventral views than in dorsal views ($p<0.0001$, Wilcoxon matched pairs
149 test, W=151, n=17). In the abdomen, we defined a rostral ("liver") region of interest (ROI) and a more
150 caudal "lower abdominal" ROI. The liver ROI accounted for 46.6 $\pm$ 3.0% (Mean ± SEM; n=17) of
151 bioluminescence from the ventral view, while the lower abdomen contributed another 38.4 $\pm$ 3.5%.
152 Bioluminescence rhythms from the throat region have previously been shown to originate in the
153 submandibular gland[51]. Bioluminescence was absent in mice with wild-type *Dbp* alleles or with the
154 conditional *Dbp*^{KI} allele (in the absence of *Cre*).

155 Post-mortem dissection and imaging revealed that tissues of the gastrointestinal tract (intestine,
156 cecum and colon), pancreas and mesenteric fat, perigonadal fat and uterus were major contributors to
157 overall light output, with liver and kidney emitting lower levels (**Fig. S2).** Organs contributing minor
158 amounts to total bioluminescence in dissected mice were esophagus, heart, lung, thymus, spleen, and testes.

159 Previous reports have shown that in a number of tissues, *Dbp* RNA levels peak earlier than *Per2*
160 RNA levels[3]. Consistent with this literature, the time of peak of bioluminescence rhythms from *Dbp*$^{Luc/+}$
161 tissues preceded the time of peak of bioluminescence rhythms from *Per2*$^{Luc/+}$ tissues by ~6 hours, both *in*
162 *vitro* (**Fig. 2C, 2F)** and *in vivo* **(Fig. 3G-3I).** Unexpectedly, bioluminescence rhythms from *Per2*$^{Luc/+}$ tissue
163 explants had significantly greater period length than explants from *Dbp*$^{Luc/+}$ mice (Lung: 25.29 $\pm$ 0.13 vs

164 23.93 ± 0.11 h; $F_{1,27.7} = 95.55$, $p < 0.0001$; Anterior Pituitary: 25.27 ± 0.08 vs 23.73 ± 0.112 h; $F_{1,24.53} =$
165 66.12, $p < 0.0001$).
166
167 **Molecular and Behavioral Rhythms in Mice with *Dbp* Reporter Alleles.** To confirm that the
168 introduction of the reporter construct into the *Dbp* locus did not alter circadian clock function, molecular
169 and behavioral rhythms were assessed. Male mice used for these analyses had either one or two copies of
170 the GFP-containing conditional allele ($Dbp^{KI/+}$ and $Dbp^{KI/KI}$, respectively), one or two copies of the
171 luciferase-expressing allele ($Dbp^{Luc/+}$ and $Dbp^{Luc/Luc}$, respectively), or were wild-type (WT) littermate
172 controls.
173 RNA was isolated from livers collected at 4-h intervals over 24-h. Northern blots were prepared
174 and probed for *Dbp* and *Actin* (loading control). As expected, the transcripts from Dbp^{KI} and Dbp^{Luc} alleles
175 migrated more slowly than the wild-type transcript (**Fig. 4A)**, due to inclusion of GFP and luciferase coding
176 sequence in these transcripts, respectively, as verified by probing for reporter sequences in a replicate blot.
177 Peak levels of *Dbp* expression in liver occurred at ZT10 in all genotypes (**Fig. 4B**), as expected based on
178 previous studies[3,42,57]. For each transcript type, the *Dbp*/*Actin* ratios were ranked within each series of 6
179 timepoints. These ranks differed significantly among the timepoints for each transcript (Friedman's One-
180 Way analysis of variance, $p < 0.002$), and post-hoc testing indicated significantly higher rankings at ZT10
181 than at ZT2, ZT18 and ZT22 (Dunn's test, $p < 0.05$). These data indicate that the temporal profile of
182 transcript expression from the *Dbp* locus was unaffected by the inclusion of reporter sequences.
183 Heterozygous mice expressed both *Dbp* and *Dbp-plus-reporter* transcripts. The two transcript types
184 did not differ in abundance: optical density over film background of the Dbp^{KI} transcript was 100.5 ± 5.3 %
185 of the Dbp^{+} transcript in $Dbp^{KI/+}$ mice (t=0.084, df=7, p= 0.94, one-sample t-test vs 100%), while the Dbp^{Luc}
186 transcript was 102.3 ± 5.0 % of Dbp^{+} transcript in $Dbp^{Luc/+}$ mice (t=0.446, df=7, p=0.669). The equivalent
187 expression level of the two transcript types in heterozygous animals strongly suggests that transcript
188 regulation and stability were not altered by inclusion of reporter-encoding sequences.

189 Potential influences of the *Dbp* reporter alleles on locomotor activity rhythms were assessed in
190 constant darkness. Mice of the same five genotypes and both sexes were examined (**Table 1; Fig. S3**). This
191 assessment was complicated by a significant sex-by-genotype interaction ($F_{4,102} = 2.904$, $p = 0.0254$) that
192 post-hoc tests indicated was the result of an unexpected sex difference in the $Dbp^{Luc/Luc}$ mice. Indeed, when
193 this genotype was excluded from the analysis, no significant sex-by-genotype interaction was observed
194 ($F_{3,88} = 1.349$; $p = 0.2636$) and one-way ANOVA demonstrated the absence of a significant main effect of
195 genotype ($F_{3,91} = 1.174$; $p = 0.3242$). One-way ANOVA within each sex with all five genotypes included
196 revealed no genotype effect in males ($F_{4,50} = 1.299$, $p = 0.283$). While there was a significant genotype
197 effect in females ($F_{4,52} = 2.716$, $p = 0.040$), Tukey HSD post-hoc tests did not find a significant result among
198 any of the pairwise genotype comparisons (all p values > 0.05). Similarly, an alternative post-hoc analysis
199 revealed that none of the other female genotypes differed from WT females in their free-running period in
200 constant darkness (Dunnett's test, p > 0.5 in each case). To further examine the effect of sex on free-running
201 period, males and females of each genotype were compared directly. In both homozygous reporter lines
202 ($Dbp^{Luc/Luc}$ and $Dbp^{KI/KI}$), males had significantly longer period lengths than females ($p < 0.01$), while this
203 was not seen in wild-type controls or heterozygous reporters ($p > 0.46$). Together, these assessments of
204 molecular and behavioral rhythms indicate that the reporter alleles do not alter circadian function or change
205 *Dbp* expression.
206
207 ***Cre*-dependent Luciferase Expression in Liver.** The main use we envision for the *Dbp* reporter alleles
208 involve *Cre* recombinase-mediated excision of GFP, leading to expression of *luciferase* in cells expressing
209 *Cre*. The effectiveness of this approach was first assessed in the liver. Hepatocytes were targeted using an
210 *Albumin-Cre*-driver line. *In vivo* bioluminescence imaging of intact *Albumin-Cre*$^{+}$; $Dbp^{KI/+}$ "liver reporter"
211 mice at the time of expected maximal bioluminescence revealed that 96.6 ± 0.48% of light originated in the
212 "liver" ROI (relative to total ventral-view bioluminescence; p<0.0001 versus 46.6 ± 3.0% in Dbp^{Luc} mice,
213 U-test, U=0, n=19 and 17, respectively). Light output from the ventral side was 5.14 ± 0.53 times greater
214 than from the dorsal view (p<0.0001, Wilcoxon matched pairs test, W=190, n=19). Notably, post-mortem

215 imaging of dissected parts confirmed that the bioluminescence signal originated exclusively from the liver
216 in these mice (97.4% of light from liver; n=12).
217 In a separate cohort of liver reporter mice, bioluminescence was assessed around the clock by IVIS
218 imaging. The cosinor-fitted time of peak of *Dbp*-driven bioluminescence rhythms from the liver 'region of
219 interest' of these mice (ZT11) was indistinguishable from the peak time of the liver ROI analyzed in whole-
220 body Dbp^{Luc} mice (**Fig. 3I**).
221
222 **Cell-type Specific Bioluminescence Rhythms in SCN Slices.** The heterogeneity of SCN neurons has
223 complicated our understanding of central clock function[58]. Neuromedin S (NMS) is expressed in ~40% of
224 SCN neurons, while Arginine Vasopressin (AVP) is expressed in ~10% of SCN neurons and is contained
225 within the NMS-expressing population[59]. The utility of our conditional reporter line was demonstrated by
226 monitoring bioluminescence rhythms within specific subpopulations of SCN neurons (**Fig. 5**). *NMS-iCre*;
227 $Dbp^{KI/+}$ mice and *AVP-IRES2-Cre;* $Dbp^{KI/+}$ mice were generated, and single-cell bioluminescence rhythms
228 were compared to those from non-conditional $Dbp^{Luc/+}$ mice in SCN slices *in vitro*. For the conditional
229 mice, bioluminescence was apparent in subsets of cells within the SCN (**Fig. 5**). The anatomical pattern of
230 bioluminescence in the SCN differed based on the *Cre* line used, consistent with the expected distribution
231 for each neuronal subtype.
232 The cell-type specificity of bioluminescence signals from the different genotypes enabled the
233 assessment of rhythm quality in the different neural populations. This assessment revealed a significantly
234 shorter period in AVP^+ neurons compared to NMS^+ cells (**Fig. 5D**; $F_{2,14.64} = 4.259$, $p = 0.0345$). Although
235 the time of peak of *Dbp*-driven bioluminescence did not differ significantly between the different cellular
236 populations examined (**Fig. 5E**; $F_{2,18.31} = 0.6570$, $p = 0.5302$), a reduction in rhythm robustness was
237 observed in AVP^+ neurons compared to rhythms of NMS^+ neurons as well as compared to all neurons (**Fig.
238 5F**; $F_{2,18.11} = 14.34$, $p = 0.0002$). In line with this reduced robustness of individual cellular oscillators, the
239 distribution of peak times was also more dispersed in AVP^+ cells compared to NMS^+ neurons (**Fig. 5G**).

240 These results complement the recent report from Shan *et al* using a Cre-dependent Color Switch
241 PER2::LUC reporter mouse demonstrating period and phase differences among sub-populations of SCN
242 neurons (AVP^+ and VIP^+), relative to the rest of the SCN[60]. Our Dbp^{KI} mice and the recently reported Color-
243 Switch PER2::LUC[60] mouse line will be important additions to our molecular/genetic armamentarium for
244 unravelling the complicated relationships among the cellular components of the central circadian
245 pacemaker in the SCN[58-64].
246
247 **Continuous, Non-invasive Detection of Bioluminescence Rhythms from Liver in Ambulatory Mice.**
248 Addressing issues of internal desynchrony and misalignment of oscillators requires monitoring the
249 dynamics of tissue resetting over time after a phase-shifting stimulus. The use of *in vivo* bioluminescence
250 imaging for repeated assessments of organ-level regions of interest over multiple days is feasible[52] but
251 requires repeated, potentially disruptive anesthesia sessions[65] per circadian cycle for several days, and
252 intensive effort by investigators. As a result, *in vivo* bioluminescence imaging has generally been relegated
253 to assessing phase of reporter gene oscillations on relatively few occasions after a shifting stimulus, with
254 rare exception[52]. An attractive alternative is to perform long-term, non-invasive bioluminescence
255 recordings, as pioneered by Saini et al.[54] who administered a virally encoded luciferase reporter by tail vein
256 injection to transduce liver, allowing bioluminescence recording from awake, behaving mice using a
257 specialized detector unit. This virally mediated reporter method is only appropriate for assessing rhythms
258 in liver, however. Other studies have attached recording devices directly to mice or used fiber optics to
259 collect light from specific brain regions in broadly luminescent *Per1-luc* or *Per2-luc* mouse reporter lines[45-
260 50,66-68], which allow monitoring rhythms from tethered but 'freely moving' mice. An elegant but more
261 invasive approach involves administering *Cre*-dependent viral reporters to mice with cell- or tissue-specific
262 *Cre* expression, allowing specific cellular populations to be monitored *in vivo*[48]. A less invasive approach
263 that allows long-term assessment of rhythms in a variety of specific tissues is desirable.
264 *In vivo* bioluminescence imaging also suffers from a lack of anatomical resolution, with the light
265 from several abdominal organs potentially merging. Tissues of the gastrointestinal tract are a major source

266 of abdominal bioluminescence in "whole-body" *(Dbp$^{Luc/+}$)* reporter mice, and these tissues likely
267 overshadow (or, more literally, out-glow) surrounding tissues, making it impossible to specifically assess
268 rhythmicity in smaller abdominal structures *in vivo*. Bioluminescence from even relatively large organs like
269 liver and kidney is likely 'contaminated' by light from the gastrointestinal tract in non-conditional reporter
270 mice.

271 To overcome these difficulties with assessing the origin of bioluminescence in "whole-body"
272 reporter mice, and to refine recently developed methods for long-term monitoring of peripheral rhythms in
273 ambulatory mice[55], we generated *Albumin-Cre*;*Dbp$^{KI/+}$* ("liver reporter") mice. First, we examined the
274 potential impact of route of substrate administration on rhythms using a Lumicycle *In Vivo* system[55]
275 (Actimetrics, Wilmette IL). Mice were entrained to 12L:12D followed by a skeleton photoperiod consisting
276 of 4 1-h pulses of light every 24 hr (1L:1D:1L:6D:1L:1D:1L:12D) with the 12-h dark phase coinciding
277 with 12-h dark phase of the preceding lighting cycle. A skeleton photoperiod was used because detection
278 of bioluminescence requires the absence of ambient light, while studies of light-induced phase shifting
279 obviously require light; a skeleton photoperiod is a compromise between these conflicting constraints. After
280 7 days in the skeleton photoperiod, mice were anesthetized for subcutaneous implantation of a primed
281 osmotic minipump (Alzet, Model #1002 (0.25µl per hour)) containing either D-luciferin (100 mM) or
282 phosphate buffered saline (PBS). Mice with PBS-containing pumps received D-luciferin in the drinking
283 water (2 mM). The time of peak of bioluminescence rhythms was determined 5 days after pump
284 implantation on the first day of exposure to constant darkness. Time of peak was determined by discrete
285 wavelet transform (DWT) analysis. There was no difference in time of peak for these routes of D-luciferin
286 administration (drinking water: mean peak time (± SEM) CT 8.75 ± 0.20 (n = 7); osmotic minipumps: mean
287 peak time CT 8.76 ± 0.19; unpaired t-test, t = 0.0342, df =12, p = 0.9733). Thus, the presumed rhythm of
288 substrate intake, secondary to the rhythm of water intake, does not change the time of peak of the
289 bioluminescence rhythm from liver reporter mice. This is consistent with recent results from Sinturel et al.
290 2021[77]. Our subsequent studies used D-luciferin (2 mM) administered in the drinking water.
291

292 **Circadian Misalignment Following a Phase Shift of the Lighting Cycle**. The approach described above
293 provides an unparalleled system for assessing the timing of rhythmicity in a specific tissue over long periods
294 of time. Thus, hepatic bioluminescence rhythms were monitored in *Albumin-Cre*; $Dbp^{KI/+}$ (liver reporter)
295 mice before and after a 6-hr phase advance of the skeleton lighting cycle described above. Control mice
296 remaining in the original (non-shifted) skeleton lighting regimen had a stable phase of hepatic
297 bioluminescence (**Fig. 6C**). In contrast, mice exposed to a phase-advance of the skeleton photoperiod
298 displayed a gradual phase-advance in both locomotor activity and hepatic bioluminescence rhythms (**Fig.**
299 **6A, B**). Notably, locomotor rhythms shifted more rapidly than hepatic bioluminescence rhythms: the liver
300 lagged behind (**Fig. 6B**). To compare the re-entrainment of bioluminescence and locomotor activity
301 rhythms, peak time for each rhythm each day was normalized to the time of peak on the last day before
302 shifting the lighting cycle in the shifted group (e.g., Day 2 in Fig. 6) for each animal. Data from each
303 lighting group were analyzed separately using a general linear model with Animal ID as a random variable
304 (allowing comparison of the two rhythms within individuals) and the main effects of the endpoint
305 (locomotor activity or bioluminescence) and Day number. In animals not undergoing a phase shift, the
306 phase relationship of these endpoints was unchanged over time ($F < 1.1$, $p > 0.39$). In contrast, in animals
307 exposed to a 6-hr phase advance of the skeleton photoperiod, the phase relationship of the locomotor
308 activity and bioluminescence rhythms differed significantly (Measure*Day interaction, $F_{9,54.98} = 3.358$, $p =$
309 0.0024). Post-hoc testing revealed a significant difference in phase between the two measures on day 9
310 (Tukey HSD, $p<0.05$). A separate analysis to compare phase (relative to Day 2 baseline) between
311 bioluminescence and locomotor activity rhythms revealed significant differences between the two measures
312 on days 5,6,7,8,9 and 10 (t-tests on each day, $p < 0.05$). Thus, both locomotor activity and hepatic
313 bioluminescence rhythms shifted following a phase shift of the lighting cycle, but the rhythms differ in their
314 kinetics of re-adjustment, with the liver lagging behind. These data provide clear evidence for misalignment
315 of SCN-driven behavioral rhythms and rhythmicity in the liver.
316

317 **Recovery from Circadian Misalignment Induced by Temporally Restricted Feeding.** We next
318 conducted a study to examine misalignment induced by restricted feeding, as previous studies have
319 shown that food availability limited to daytime significantly alters phase of peripheral
320 oscillators[35,54]. Due to our desire to study bioluminescence rhythms without interference from the
321 light-dark cycle, our experiment assessed the timing of the *Dbp*-driven liver bioluminescence
322 rhythms in constant darkness after different feeding regimens were administered in a light-dark
323 cycle. This allowed us to determine the time of peak bioluminescence of the liver after restricted
324 feeding, and the unprecedented opportunity to observe its return toward a normal phase
325 relationship with SCN-driven behavioral rhythms over time in constant darkness with *ad libitum*
326 food access.

327 *Alb-Cre;Dbp*$^{KI/+}$ liver reporter mice were exposed to one of three feeding regimes (*ad*
328 *libitum*, nighttime, or daytime food availability; **Fig. 7A**) for ten days preceding bioluminescence
329 recording in constant darkness under *ad libitum* feeding conditions. A previously described
330 automated feeder system[69] was used to restrict food availability. This system limits total daily
331 consumption (to prevent hoarding). With the setting used, this system restored daily food
332 allotments to *ad libitum* fed and night-fed mice daily at 0000h (ZT18), and restricted food pellet
333 delivery for day-fed mice to 0600-1800 h (ZT0-ZT12), and for night-fed mice to 1800-0600 h
334 ZT12 – ZT24/0). This midnight food replenishment resulted in unusual temporal profiles of food
335 intake in *ad libitum* and night-fed mice. Nevertheless, *ad libitum* and nighttime food access both
336 resulted in food intake being concentrated in the night while daytime food availability resulted in
337 the midpoint of daily food intake occurring during the first half of the light phase (**Fig. 7A, 7C**).
338 Within-group variability in the timing of food intake was low except for three clear outliers (**Fig.**
339 **7C**) that were excluded from subsequent analyses.

340 *Ad libitum* fed mice showed consistently phased rhythms in bioluminescence after transfer
341 to constant darkness from 12h L:12h D, as did night-fed animals (**Fig. 7A, 7D**). In contrast, mice
342 fed only during the light period for 10 days prior to housing in DD with *ad libitum* food had an
343 earlier time of peak of the hepatic bioluminescence rhythm. Daytime feeding resulted in a
344 significantly advanced peak time compared to both night-fed and *ad libitum* fed mice, while these
345 latter groups were statistically indistinguishable ($F_{2,259.6} = 76.66$, $p < 0.0001$; **Fig. 7D**). Subsequent
346 exposure to constant darkness with *ad libitum* feeding allowed the hepatic clock of day-fed mice
347 to return toward the appropriate phase relationship with the locomotor activity rhythm regulated
348 by the SCN circadian pacemaker.

349 Although daytime feeding resulted in an advanced time of peak bioluminescence, the
350 timing of the liver bioluminescence rhythm was not solely controlled by the timing of food intake.
351 First, no significant correlations between the timing of food intake and time of peak
352 bioluminescence were observed within any of the three feeding regimes ($F < 1.13$, $p > 0.32$; **Fig.**
353 **7C**). Second, the relationship between the timing of liver bioluminescence rhythms relative to the
354 midpoint of food intake was significantly different between the different groups ($F_{2,17} = 313.2$, p
355 < 0.0001; **Fig. 7E**). While *Dbp*-driven hepatic bioluminescence rhythms were roughly in anti-
356 phase with the midpoint of feeding in *ad libitum* and night-fed mice, daytime feeding resulted in
357 near synchrony between these different rhythms (**Fig. 7E**). Furthermore, although the average
358 midpoint of feeding was significantly earlier in night-fed compared to *ad libitum* fed mice ($t_{10} =$
359 6.21, $p < 0.0001$; **Fig. 7C**), no significant difference was observed in bioluminescence phase
360 relative to the preceding light-dark cycle (**Fig. 7D**), with the timing of liver bioluminescence
361 rhythms relative to the midpoint of food intake being significantly delayed in night-fed compared
362 to *ad libitum* fed mice (**Fig. 7E**). Overall, these results demonstrate that although the timing of

363 food intake strongly influences liver rhythms, the timing of bioluminescence rhythmicity in liver
364 reporter mice is not solely driven by the timing of food intake (with food intake regulated for this
365 duration and in this way).
366
367 **Discussion**
368 Numerous studies have made use of rhythmically expressed bioluminescent reporter genes
369 to monitor circadian rhythms. The *Per2*^{Luc} mouse has been especially useful as it generates robust
370 bioluminescence rhythms from numerous tissues *in vitro*. The widespread expression of
371 PER2::LUC (and other 'non-conditional' bioluminescence reporters) comes at a cost, however, as
372 it is not possible to assess rhythmicity in specific cell populations within a larger tissue without
373 dissection. Tissue explant preparation can cause phase-resetting, however, especially after
374 exposure to phase shifting stimuli[70,71]. Furthermore, *ex vivo* culturing of tissues does not allow
375 assessment of rhythmicity in the context of the hierarchical circadian system or dynamic changes
376 during environmentally-induced resetting.
377 We chose to modify the *Dbp* gene to generate a conditional reporter for several reasons.
378 *Dbp* is widely and rhythmically expressed at readily detectable levels in numerous tissues[3,57]. This
379 feature ensures that the reporter mouse would be useful for detecting rhythmicity in numerous
380 tissues. In addition, individual clock genes are responsive to different signaling pathways. This
381 differential regulation can lead to circadian misalignment *within* the circadian clock[39,43]. As an
382 output gene, *Dbp* rhythmicity is likely a good proxy for the integrated output of the molecular
383 clockwork in total. Finally, concern that the targeting event could disrupt function of the modified
384 gene led us to steer away from core clock genes. For example, the GFP-expressing *Dbp* transcript
385 lacks the native 3′ UTR and uses an exogenous polyadenylation sequence, which could affect *Dbp*

386 gene expression and regulation. Notably, however, our Northern blot analysis suggests little or no
387 alteration in expression level or dynamics of the reporter transcripts; an observation in line with
388 the previous finding that mice homozygous for a targeted allele of *Dbp* have only a modest
389 circadian phenotype[72].

390 Shan et al.[60] recently reported development of a Color-Switch PER2::LUC line which they
391 used to demonstrate the utility of a Cre-dependent reporter approach for interrogating SCN
392 circuitry. The Color-Switch PER2::Luc line has the advantage of reporting on both Cre-positive
393 and Cre-negative cells in different colors. This strength of the Color-Switch PER2::LUC reporter
394 can simultaneously be a weakness, in that detection of bioluminescence requires segmentation of
395 the bioluminescence signal between wavelengths. Our 'simpler' approach of only inducing a
396 bioluminescence signal in *Cre*-positive cells of $Dbp^{KI/+}$ mice enables recording of bioluminescence
397 rhythms without the need for wavelength segmentation. In addition, the *Dbp* reporter can easily
398 be used in *Per2* mutant mice. Like the Color-Switch PER2::LUC line, our *Dbp* conditional reporter
399 line is useful for *ex vivo* studies, allowing specific cellular populations to be monitored by crossing
400 to the appropriate *Cre*-expressing lines. Our studies reveal subtle differences among the population
401 of oscillators defined by AVP-*Cre*, NMS-*Cre*, and the entire SCN cohort. More specifically, AVP
402 cells had a shorter period, reduced rhythmicity index, and larger within-slice dispersal of peak
403 times than the NMS cell population with which it overlaps. Our results suggest that AVP cells are
404 coordinated less well and are less robust, in contrast to the typical view of AVP cells as high-
405 amplitude 'output' neurons that also contribute to determination of period and rhythm amplitude[58].

406 We envision this line being very useful for monitoring additional neuronal subpopulations
407 in the SCN in wild-type and mutant animals. Additional technical development may allow *in vivo*
408 detection of bioluminescence rhythms from neuronal populations in awake behaving mice.

409 Approaches to optimize the signal detected from brain include use of highly efficient and cell- and
410 brain-penetrant substrates[73,74], cranial windows[75] and hairless or albino mice[55,74]. These
411 approaches may allow interrogation of the SCN circuit *in vivo*, extending the elegant studies being
412 performed with SCN slices *in vitro.* Bioluminescence rhythms can also be examined in neuronal
413 populations outside the SCN, by using an appropriate *Cre* driver and/or viral delivery of *Cre*
414 recombinase.

415 *In vivo* bioluminescent imaging allows assessment of bioluminescence from several organs
416 *in vivo*, but the signal from these areas likely includes light emitted from nearby organs (e.g.,
417 intestinal tract and abdominal fat likely contribute to the signal attributed to liver and kidney).
418 Indeed, the size and shape of the "liver" ROI seen by IVIS imaging differs between *Dbp* liver
419 reporter mice and whole-body reporter Dbp^{Luc} mice. Furthermore, bioluminescence from nearby
420 tissues can be obscured by the high level of light output coming from liver, kidney and intestines.
421 *Cre*-mediated recombination of the conditional *Dbp* reporter allele thus enables assessment of
422 bioluminescence from other tissues.

423 *Cre*-mediated recombination of the Dbp^{KI} allele in liver enabled us to perform continuous,
424 *in vivo* bioluminescence monitoring of liver in freely moving mice. These studies demonstrate
425 transient misalignment between the liver oscillator and SCN-regulated behavioral rhythms.
426 Repeated misalignment among oscillators is thought to contribute to adverse metabolic and health
427 consequences of chronic circadian disruption. Up until now, technical and practical limitations
428 have restricted our ability to monitor the behavior of circadian rhythms in different peripheral
429 tissues during and following environmental disruption of circadian homeostasis. Our *Cre*-
430 conditional reporter line and the approaches described here for assessing bioluminescence rhythms
431 *in vivo* will allow longitudinal and tissue-specific characterization of misalignment and recovery

432 after a variety of circadian-disruptive lighting and food availability paradigms, allowing more
433 extensive testing of the consequences of repeated misalignment of peripheral clocks.

434 Previous studies have shown misalignment between central and peripheral clocks induced
435 by altering the time of food access to daytime, by assessing oscillator phase at various time-points
436 after a phase shift of the lighting cycle, or by exposure to non-24hr light-dark schedules. The vast
437 majority of these studies monitored bioluminescence rhythms *ex vivo* or assessed transcript levels
438 following tissue collection at various times after a shift[29-36,37-41,69]. Notably, *ex vivo*
439 bioluminescence rhythm timing may be affected by prior lighting conditions[70,71]. Few studies have
440 followed bioluminescence rhythms *in vivo* over time after a light-induced phase shift or after a
441 food manipulation that phase-shifts peripheral oscillators[52,76]. Our current data leverage the
442 unprecedented ability to non-invasively monitor rhythmicity from a peripheral oscillator in
443 individual animals over many days to show the time course of internal misalignment and recovery
444 after a phase shift. Other studies with minimally invasive monitoring of bioluminescence rhythms
445 have relied upon viral introduction of the reporter into liver, and thus are limited to studies of
446 liver[54,77]. Moreover, efficient expression of virally delivered reporter constructs is limited by the
447 promoter size and specificity. Future studies of additional tissues in *Cre*-conditional reporter mice
448 will enable a full deciphering of how other components within the hierarchical, multi-oscillatory
449 circadian system respond to disruptive stimuli. Several studies suggest that organs differ in their
450 response to resetting stimuli. For example, the *Dbp* mRNA rhythm in liver is more fully reset than
451 the rhythm in heart and kidneys 3 days after restricting food availability to daytime[38], and several
452 studies indicate the SCN (and the locomotor rhythms it regulates) reset more rapidly than
453 peripheral tissues[21,30-33,38,43,50,52,54].

454 A further advance in studying the behavior of peripheral oscillators is provided by the
455 ability to temporally regulate the timing of feeding. A recent study[76] used a feeding device similar
456 to the one used here to recapitulate food intake patterns in mice with restricted food access that
457 were more naturalistic than the severe 'all or none' patterns typically used in studies with time-
458 restricted access to food. The authors found that peripheral oscillators of *Per2*^{Luc} mice were not
459 effectively entrained by these imposed 'natural' feeding patterns. Similarly, our restricted food
460 access study produced a smaller and more variable phase shift of the hepatic circadian clock (as
461 indicated by the initial time-of-peak of *Dbp*-driven bioluminescence) than expected based on
462 published results using presence / absence food availability cycles. A longer period of adjustment
463 to the restricted feeding schedule or more complete and abrupt transitions between food presence
464 and absence would likely produce a stronger entraining signal for the liver. Use of a variety of
465 different *Cre* drivers will allow assessment of whether different peripheral organs respond
466 similarly to food restriction paradigms. In addition, tissue-specific reporter models will be very
467 useful in assessing how more naturalistic food ingestion paradigms influence peripheral circadian
468 clocks in several tissues. These approaches will characterize circadian organization in normal and
469 disruption paradigms, helping to identify factors contributing to the adverse consequences of
470 circadian disruption.
471

472 **Materials and Methods**

473 **Animals and Housing Conditions**

474 All animal procedures were reviewed and approved by the Institutional Animal Care and Use
475 Committees of the University of Massachusetts Medical School, Morehouse School of Medicine, the
476 University of Warwick, and/or Smith College.

477 Unless otherwise noted, animals were maintained in a 12h light: 12h dark (LD) lighting cycle with
478 access to food (Prolab Isopro RMH3000; LabDiet) and water available *ad libitum*. Zeitgeber Time (ZT)
479 refers to time relative to the lighting cycle. ZT 0-12h is the light phase and ZT 12-24h is the dark phase.

480 *Cre* recombinase-expressing lines were obtained from the Jackson Labs and were crossed to mice
481 bearing the conditional (Dbp^{KI}) reporter allele to generate mice expressing luciferase in specific cells or
482 tissues. The following tissue-specific *Cre* lines were used:
483 *Albumin-Cre* (B6.Cg-$Speer6\text{-}ps1^{Tg(Alb\text{-}Cre)21Mgn}$/J ; JAX 003574), *AVP*-IRES2-*Cre* (B6.Cg-$Avp^{tm1.1(Cre)Hze}$/J;
484 JAX 0023530), and *NMS-Cre* (Tg(Nms-iCre)^{20Ywa}, JAX 027205). These lines direct Cre recombinase
485 expression to hepatocytes, neurons expressing arginine vasopressin (AVP), and neurons expressing
486 neuromedin S (NMS), respectively. In addition, a *Prrx1-Cre* female (B6.Cg-Tg(Prrx1-Cre^{1Cjt}/J), JAX
487 005584) was used for germline deletion of the conditional allele (see below). All *Cre*-expressing lines were
488 on the C57BL/6J background.

489 Founder $Per2^{Luc/+}$ mice with an in-frame fusion of firefly luciferase to PER2, and an SV40
490 polyadenylation signal[19,78] were generously provided by Dr. Joseph Takahashi, University of Texas
491 Southwestern Medical School, Dallas. This line was maintained by backcrossing to C57BL/6J mice (JAX
492 000664). All $Per2^{Luc}$ reporter mice used for experiments here were heterozygous (e.g., $Per2^{LucSV/+}$).

493 **CRISPR/Cas9 targeting the *Dbp* locus**

494 The mutant allele was generated by CRISPR/Cas9 mediated engineering of the *Dbp* locus. The targeting
495 construct consisted of a 5′ homology arm terminating just 5′ of the *Dbp* stop codon followed by in-frame
496 sequences encoding a T2A linker, LoxP, GFP with the bovine growth hormone polyadenylation signal,
497 LoxP, and Luc2 followed by the 3′-UTR of *Dbp* (3′ homology arm). Two sets of injections were done. In
498 the first injection set, which led to 17 mice, C57BL/6J blastocysts were microinjected with the donor
499 construct, and 20 ng/ul of each of two guide RNAs (MmDBPki_gR49f 5′
500 GCCCAGCAUGGGACACUGUG 3′ and MmDBPki_gR69f 5′ AGGCCACCUCCACCCUGCCA 3′).
501 This set of injections did not lead to any putative founders. For the second set of microinjections, blastocysts

502 were injected with 40 ng/ul guide RNA MmDBPki_gR49f, 50 ng/ul *Cas9* mRNA (synthesized from a Cas9
503 PCR product using mMessage mMachine T7 Ultra Kit from Life Technologies) and 20 ng/ul CAS9 protein
504 (IDT). From 34 mice generated in this set, two putative founders were identified using a primer pair internal
505 to the construct (primer pair C, see **Table S1**). Primer pairs consisting of a primer in flanking DNA, external
506 to the construct, and a primer within the construct were used to confirm that one of these animals had the
507 desired targeting event (primer pairs F and H, which spanned the 5′ and 3′ ends, respectively). Genomic
508 DNA from this mouse was then amplified using a primer pair flanking the entire construct; sequencing the
509 product confirmed the construct was inserted properly, *in vivo*. The founder carrying the targeted (knock-
510 in or Dbp^{KI}) allele and its offspring were backcrossed to C57BL/6J mice (JAX 000664) for three generations
511 before any intercrossing to reduce off-target mutations.

512 To generate mice with germline deletion of GFP (and thus leading to expression of luciferase
513 throughout the body), a male $Dbp^{KI/+}$ was bred to a *Prrx1-Cre* female (JAX 005584), which we had on hand
514 and which produces germline deletion of floxed alleles at high frequency. Several mice bearing the newly
515 generated Dbp^{Luc} allele were identified and backcrossed to C57BL/6J, selecting against *Prrx1-Cre*.

516 **Genotyping**

517 Genotyping was performed by PCR amplification of DNA extracted from ear punches.
518 Amplification products were separated by agarose gel electrophoresis. Genotyping protocols for *Cre*
519 recombinase and $Per2^{Luc}$ have been published previously[53, 79]. A primer set ("4A") capable of detecting all
520 possible *Dbp* allele combinations was used for colony genotyping; the three possible alleles (Dbp^{+}, Dbp^{KI},
521 Dbp^{Luc}) generate amplicons of different size with this primer set (299, 399 and 490 bp, respectively). Primer
522 sets are listed in **Table S1**.

523 **Generation of Digoxigenin (DIG) DNA Probes and Northern Blot Assay**

524 DIG-labeled DNA probes were generated by PCR in reactions containing 28 μM of DIG-labeled
525 UTP following the manufacturer's protocol (Roche). Primer sets are listed in **Table S1**.

526 WT, *Dbp*$^{KI/+}$, *Dbp*$^{KI/KI}$, *Dbp*$^{Luc/+}$, and *Dbp*$^{Luc/Luc}$ mice were euthanized by Euthasol injection and liver
527 tissue was collected at 4-h intervals (ZT 2, 6, 10, 14, 18, 22). RNA was isolated from the liver tissue by
528 Trizol extraction (Ambion). RNA was quantitated by Nanodrop. Five micrograms per lane were separated
529 by electrophoresis on a 1.2% formaldehyde gel. RNA was transferred to a nylon membrane and cross-
530 linked by UV exposure. Blots were prehybridized, probed and detected following the manufacturer's
531 protocol (Roche), bagged and exposed to X-ray film.

532 **Locomotor Activity Rhythms**

533 Male and female mice of five genotypes (WT, *Dbp*$^{KI/+}$, *Dbp*$^{KI/KI}$, *Dbp*$^{Luc/+}$, and *Dbp*$^{Luc/Luc}$) were
534 transferred to the experimental room and single-housed with a running wheel. Animals had access to food
535 and water *ad libitum*. Running-wheel activity was monitored using ClockLab collection software
536 (Actimetrics). Mice were entrained to a 12-h light/12-h dark cycle for 18 days, then were placed into
537 constant darkness (dim red light) for 15 days. The free-running period for each animal was determined on
538 days 4-15 in DD by periodogram analysis using ClockLab analysis software.

539 **Bioluminescence Recordings from Tissue Explants**

540 Tissue explants were prepared late in the afternoon from *Per2*$^{Luc/+}$ and *Dbp*$^{Luc/+}$ mice housed on a
541 12-h light/12-h dark lighting cycle. Mice were deeply anesthetized with Euthasol and decapitated. Tissues
542 were dissected and immediately placed in ice-cold 1X HBSS (Gibco). Pituitary gland was subdivided into
543 4 sections (~2mm^3) with a scalpel and each piece was cultured separately. Lung explants were placed three
544 per dish. Up to three replicate dishes were studied per tissue per animal. Explants were placed on sterile
545 35-mm Millicell culture plate inserts (Millipore) in a sealed petri dish containing air-buffered
546 bioluminescence medium [53,80] plus D-luciferin (100 μM) (Gold Biotechnology) and incubated at 32 °C.
547 Bioluminescence was measured from each dish for 1 minute every 15 minutes using a Hamamatsu LM-
548 2400 luminometer.

549 Bioluminescence records were analyzed to determine period and peak time. The first 12-h were
550 discarded to exclude acute responses to explant preparation. Photon counts were smoothed to a 3-h running
551 average and baseline subtracted using a 24-h running average. Circadian period was determined from the

552 average of the period between each peak, trough, upward crossing and downward crossing between 24 and
553 88 hr of recording for each record. Peak time was calculated as the clock time of the first peak in the
554 background-subtracted data. Tissues from mice of the two genotypes were studied together in each run.

555 **Imaging of *In Vivo* Bioluminescence Rhythms**

556 *In vivo* imaging was performed in the UMass Medical School Small Animal Imaging Core Facility
557 using an In Vivo Imaging System (IVIS-100, Caliper, now Perkin Elmer) as previously described[52,53]. *Alb-*
558 *Cre*$^{+}$*; Dbp*$^{KI/+}$, *Dbp*$^{Luc/+}$, and *Per2*$^{Luc/+}$ mice were anesthetized with 2% isoflurane (Zoetis Inc.) and skin
559 covering the liver, kidneys and submandibular glands was shaved. Mice were injected with D-luciferin (i.p.,
560 100 µl at 7.7 mM, Gold Biotechnology) and Dorsal (9 min post-injection) and Ventral (10.5 min post-
561 injection) images were captured from each animal. To assess bioluminescence rhythms, anesthesia, D-
562 luciferin injection and imaging was repeated at 4- to 8-hour intervals over approximately 30 hours.
563 Experiments to localize the source of bioluminescence utilized a single injection of D-luciferin at the time
564 of the expected peak bioluminescence, followed by euthanasia, dissection, and *ex vivo* imaging.

565 IVIS images were analyzed using Caliper Life Sciences' Living Image software (version 4.4).
566 Bioluminescence within Regions of Interest (ROI) of fixed size for all time-points in each mouse was
567 determined and analyzed as previously described[53].

568 **Assessing Distribution of Bioluminescence *In Vivo* and *Ex Vivo***

569 Whole-body reporters (*Dbp*$^{Luc/+}$) and liver reporters (*Alb-Cre+;Dbp*$^{KI/+}$) were used to assess the
570 distribution of bioluminescence by IVIS imaging. Mice were anesthetized with isoflurane, shaved, and
571 injected with D-luciferin (100 microliters at 7-10 mM, i.p.) at times of peak expression (ZT 11-16). Images
572 were captured of ventral and dorsal views at 9-12 minutes after injection.

573 Bioluminescent counts within regions of interest (ROIs) were calculated using Living Image 4.4
574 software. ROIs identified on the ventral surface were the whole rectangular region containing the mouse,
575 and sub-ROI's where a region in the throat (submandibular gland), upper abdomen, and lower abdomen,
576 and any other hot-spots observed. Dorsal ROI's were the rectangle containing the entire mouse and a sub-

577 ROI over the lower back, corresponding to the abdomen on the dorsal side. Subsequent calculations were
578 performed in Microsoft Excel.

579 Animals were euthanized while under anesthesia, and organs were dissected and imaged to assess
580 the distribution of light. Due to the time required for sequential dissection and image capture of multiple
581 animals, some images of dissected tissues were captured as long as 60 minutes after D-luciferin injection,
582 and up to 10 minutes after euthanasia. Preliminary studies conducted by capturing images at various time
583 after euthanasia suggested there is no change in the distribution of bioluminescence with time, although
584 absolute levels fall with time. These studies indicated significant contribution of bioluminescence from
585 small intestine, colon, cecum, pancreas and mesenteric fat, uterus and perigonadal fat, with liver and kidney
586 emitting less light. Thymus, heart, lung and spleen contributed very little light output under the imaging
587 conditions used.

588 **Bioluminescence Imaging of SCN Explants**

589 Coronal sections containing SCN from *NMS-Cre;Dbp*$^{KI/+}$, *AVP-IRES-CRE;Dbp*$^{KI/+}$, and *Dbp*$^{Luc/+}$
590 mice were dissected, cultured, and imaged as previously described[81,82]. Briefly, sections containing SCN
591 (150 μm) were collected from adult mice, cultured on a membrane (Millicell CM; Millipore) in 1.2 mL of
592 air-buffered media containing 100 μM D-luciferin (Gold Biotechnology), and imaged for 5 days using a
593 Stanford Photonics XR/MEGA-10Z cooled intensified charge-coupled device camera.

594 Rhythmic parameters of luciferase expression were calculated for each slice and for cell-like
595 regions of interest (ROIs) within each slice using computational analyses in MATLAB (R2018a,
596 MathWorks) as described previously[82,83]. Briefly, to locate and extract data from cell-like ROIs, we
597 employed an iterative process identifying clusters of at least 20 bright pixels after background and local
598 noise subtraction (through application of a 2D wavelet transform using Wavelab 850,
599 (https://statweb.stanford.edu/~wavelab/) of a slice image summed across 24 h of bioluminescence. To
600 extract time series for the ROI's, each image in the sequence was smoothed via convolution with a Gaussian
601 kernel applied to 12x12-pixel regions and reduced from 512x640 resolution to 256x320. A discrete wavelet
602 transform (DWT) was applied to each time series to remove the trend and to extract the circadian and noise

603 components using the *wmtsa* toolbox for MATLAB (https://atmos.uw.edu/~wmtsa/). The criteria for
604 circadian rhythmicity in the ROI time series were a peak autocorrelation coefficient of at least 0.2, a
605 circadian component peak-to-peak time between 18 and 30 h, an amplitude above baseline noise (standard
606 deviation of noise component), and a cross-correlation coefficient of at least 0.4 with an aligned sine wave
607 over a 48h window. Peaks of the DWT circadian component were used to estimate peak time of each ROI.

608 Rhythmicity index (RI) is the peak in the autocorrelation of the DWT-detrended time series,
609 corresponding to a lag between 16 and 36 hrs, as previously described[84,85]. The time of peak
610 bioluminescence, rhythmicity index and the scatter of peak times within each slice for each ROI was
611 assessed on the first day *in vitro*. Period of rhythmicity in each ROI was determined as the average peak-
612 to-peak interval in the second and third cycles. These measures were compared between genotypes by a
613 general linear model, with slice ID included as a random variable to account for multiple cells being
614 measured on each slice. Where applicable, post-hoc comparisons were performed using Tukey's HSD
615 pairwise comparisons.

616 **Bioluminescence Rhythms in Ambulatory Liver Reporter Mice**

617 Bioluminescence was measured in freely moving *Alb-Cre*$^{+}$ *; Dbp*$^{KI/+}$ reporter mice with the
618 "Lumicycle *In Vivo*" system (Actimetrics, Wilmette, IL) using methods as recently described[55]. Each unit
619 contained two PMTs (Hamamatsu H8259-01), and programmable LED lights. A programmable shutter
620 blocked the PMTs during periods of light exposure and to measure 'dark counts'. Each 1-minute dark-count
621 value was subtracted from the counts recorded during the subsequent 14 minutes to obtain the background-
622 corrected count values, to compensate for the effect of temperature fluctuations on PMT signal. Locomotor
623 activity was recorded using passive infrared motion sensors (Visonic, K940) and Clocklab software
624 (RRID:SCR_014309). Animals were checked daily at varied times using an infrared viewer (Carson
625 OPMOD DNV 1.0), or goggles (Pulsar Edge Night Vision Goggles PL75095).

626 **Analysis of Ambulatory Bioluminescence Rhythms.** Ambulatory bioluminescence data were
627 analyzed using RStudio. A discrete wavelet transform (DWT) was applied to each time series to detrend
628 and to calculate the time of peaks using the wmtsa R package (https://cran.r-

629 project.org/web/packages/wmtsa/index.html), as described[83-85]. The S12 filter was applied on 15-min
630 median binned data; medians were used (instead of means) to reduce the effect of large outliers. Data before
631 the first trough and after the last trough were discarded to avoid edge effects.

632 **Assessing Routes of Administration of Luciferin.** To determine whether rhythmic substrate
633 intake influences the pattern of bioluminescence, we compared the time of peak bioluminescence between
634 animals receiving continuous administration of substrate (from a subcutaneous osmotic minipump) with
635 trials in which mice received D-luciferin in the drinking water (2 mM) and implantation of a PBS-filled
636 osmotic pump.

637 Liver reporter mice previously housed in 12L:12D were entrained to a skeleton photoperiod (SPP)
638 consisting of four 1-hour light pulses. A skeleton photoperiod provides additional periods of darkness in
639 which to record bioluminescence. In the SPP, illumination occurred in four 1-hour blocks within the light
640 phase in the preceding lighting cycle (e.g., lights were on from ZT 0-1, 2-3, 9-10, and 11-12, so the first
641 and last hours of light in SPP coincided with light onset and offset, respectively, in the full photocycle with
642 lights on ZT0-12 and lights off ZT12-24/0). On the seventh day of SPP entrainment, mice were given
643 analgesics (0.05 mg/kg Buprenorphine and 2.0 mg/kg Meloxicam), anesthetized with 3% isoflurane, shaved
644 from hips to shoulders, and a primed osmotic minipump (Alzet Model #1002, 0.25µl per hour, 14 day)
645 containing D-luciferin (100 mM dissolved in PBS) or PBS vehicle was implanted subcutaneously. Mice
646 were returned to their cages with a warming disc and were provided soft food during the first 24 hours of
647 recovery. Animals were placed into the LumiCycle *In Vivo* unit 2.5 days after surgery. Bioluminescence
648 was recorded in SPP lighting for 2.5 days, then lights were disabled at the time of lights-out. The time of
649 peak bioluminescence was determined by wavelet analysis on the first day in constant darkness. No
650 difference in peak time of bioluminescence was found (see Results); in subsequent studies we administered
651 D -luciferin (2 mM) in the drinking water.

652 **Re-entrainment following a Phase Shift of the Skeleton Photoperiod.** Additional studies were
653 conducted to assess re-entrainment of the bioluminescence rhythms after a 6-hr advance of the light-dark
654 cycle. Animals previously entrained to a full 12L:12D lighting cycle were transferred to the skeleton

655 photoperiod described above for several days before study. Mice were anesthetized with isoflurane and
656 shaved 2.5 days prior to placement in the LumiCycle *In Vivo* units. D-Luciferin (2 mM) was provided in
657 the drinking water. Skeleton photoperiod lighting conditions were either maintained at the initial pattern or
658 advanced by 6 hr after the second day of recording. Locomotor activity was detected by passive infrared
659 motion sensors.

660 **Analysis**. The circadian time of peak bioluminescence and the mid-point of locomotor activity
661 were determined by wavelet analysis on each day of recording. For studies of phase shifts in response to
662 shifting the skeleton photoperiod, the timing of bioluminescence rhythms and locomotor activity rhythms
663 were normalized relative to the timing of these rhythms on Day 2 (e.g., the last day before shifting the
664 lighting cycle in the shifted group) for each animal. Data are expressed as mean ± SEM for each genotype
665 and endpoint on each day. Data from each lighting group were analyzed separately using a general lineal
666 model with Animal ID as a random variable (allowing comparison of the two rhythms within individuals)
667 and the main effects of the endpoint measure (locomotor activity or bioluminescence) and Day number,
668 and the 2-way interaction Measure*Day. In animals not undergoing a phase shift, potential changes in the
669 timing of the locomotor or bioluminescence rhythm were assessed separately for either measure by testing
670 the influence of Day number.

671 **Food Restriction Followed by Bioluminescence Recording.** Liver reporter mice (*Albumin-Cre;*
672 $Dbp^{KI/+}$) were fed pellets (300 mg, Dustless Precision Pellets, Rodent, Grain-Based, F0170, BioServ,
673 Flemington, NJ, USA) through the Actimetrics timed feeding apparatus designed by Phenome
674 Technologies, Skokie, IL, USA. Pellets were spaced by a minimum of 10 minutes to prevent hoarding
675 behavior[69]. Three groups were studied: those with *ad libitum* access to food, those with feeding restricted
676 to the light phase of the LD cycle (daytime feeding), and mice with access to food restricted to the dark
677 phase of the LD cycle (nighttime feeding). Mice were held under their feeding regime for 10 days prior to
678 bioluminescence recording. They were weighed regularly to ensure body weight did not decrease below
679 95% of initial weight. All mice were kept on a 12L:12D lighting schedule during the period of food
680 manipulation, and then were released into constant darkness for bioluminescence recording. During the LD

681 period, data were collected on feeding, light levels, and locomotor behavior (using motion sensors). Three
682 days before entering the Lumicycle In Vivo units, cage bottoms were changed at dark onset. *Ad libitum* and
683 night-fed mice were placed into the LumiCycle In Vivo units at dark onset with food immediately available.
684 Day-fed mice were placed into the LumiCycle In Vivo units at dark onset but were provided food after 12
685 hours (at the time of light onset in the previous LD cycle) to continue the daytime feeding regime during
686 the first day of the recording period. Bioluminescence was recorded for 7 days.

687 Liver reporter animals were randomly assigned to treatment groups and recording boxes.
688 Experimental groups and controls ran in parallel over five cohorts lasting 3 months. 24 hours prior to
689 placement in the recording boxes, mice were shaved from hips to shoulders on their front and back under
690 3% isoflurane and returned to their cages. 6 hours prior to placement into the in vivo boxes, mice were
691 provided with D-luciferin (2mM) in the drinking water to enable instantaneous bioluminescence upon
692 recording onset.

693 **Analysis.** For each animal the center of gravity (COG) of food intake was calculated for the last 5
694 days of the feeding regimen. Food intake patterns were also independently assessed qualitatively by four
695 observers. These assessments led to identification of three cohorts of mice, based on food intake patterns.
696 Three mice were identified as clear outliers compared to these three cohorts based on visual inspection of
697 the food intake timing. In line with this qualitative assessment, the feeding COG of each of these 3 animals
698 was >2 h removed from the other animals in their cohort (**Fig. 7C**). These three animals were excluded
699 from cohort-based assessments. Peak of bioluminescence on each day was calculated by DWT analysis as
700 above. Missing data resulted from inability to define a time of peak on some days. Hair regrowth contributed
701 to loss of signal and loss of rhythm amplitude, and thus to missing data in some cases.
702

703 **Acknowledgments**

704 We thank Christopher Lambert and Jamie Black for technical assistance, and Steven A. Brown
705 (University of Zurich) for discussions and encouragement in the development of this project.
706 Use of UMass Medical School core facilities (Mutagenesis Core, Mouse Modeling Core, and Small Animal
707 Imaging Core) is gratefully acknowledged.

708 Research reported in this publication was supported by the National Institute for Neurological
709 Diseases and Stroke and the National Institute of General Medical Sciences of the National Institutes of
710 Health under award numbers R21NS103180 (DRW), SC1GM112567 (AJD), and NIGMS R15GM126545
711 (MEH), the Hartmann Müller Stiftung (RD), MRC MC_PC_15070 (RD) and BSN (RD and LAG). CBS
712 was a participant in the UMass Medical School Initiative for Maximizing Student Development, supported
713 by NIH grant R25GM113686. The funders had no role in study design, data collection and analysis,
714 decision to publish, or preparation of the manuscript. The content is solely the responsibility of the authors
715 and does not necessarily represent the official views of the National Institutes of Health or the other funding
716 agencies.

717

718 **Author Contributions**

719 R.D and D.R.W. conceived the project
720 C.B.S., V.v.d.V., E.M., M.H.B., A.J.D., M.E.H., R.D. and D.R.W. designed research
721 C.B.S., V.v.d.V., E.M., A.C.S., B.M.B., P.C.M., L.A.G., R.D., and D.R.W. performed research
722 C.B.S., V.v.d.V., E.M., T.L.L., B.M.B., M.E.H., R.D. and D.R.W. analyzed data
723 C.B.S., V.v.d.V., and D.R.W. wrote the paper
724 All authors have approved this version of the manuscript.

725 **References**

726

727 1. S. M. Reppert, D. R. Weaver, Coordination of circadian timing in mammals. *Nature* **418**, 935–941
728 (2002).
729 2. J. A. Mohawk, C. B. Green, J. S. Takahashi, Central and peripheral circadian clocks in
730 mammals. *Annu Rev Neurosci* **35**, 445–462 (2012).
731 3. R. Zhang, N. F. Lahens, H. I. Ballance, M. E. Hughes, J. B. Hogenesch, A circadian gene expression
732 atlas in mammals: implications for biology and medicine. *Proc Natl Acad Sci U S A* **111**, 16219–
733 16224 (2014).
734 4. A. Patke, M.W. Young, S. Axelrod, Molecular mechanisms and physiological importance of
735 circadian rhythms. *Nat Rev Mol Cell Biol* 21(2): 67-84 (2020).
736 5. J. A. Evans, A. J. Davidson, Health consequences of circadian disruption in humans and animal
737 models. *Prog Mol Biol Transl Sci* **119**, 283–323 (2013).
738 6. D.M. Arble, *et al*., Impact of sleep and circadian disruption on energy balance and diabetes: A
739 summary of workshop discussions. *Sleep* **38**, 1849-1860 (2015).
740 7. A. C. West, D. A. Bechtold, The cost of circadian desynchrony: Evidence, insights and open
741 questions. *Bioessays* **37**, 777–788 (2015).
742 8. T. Roenneberg, M. Merrow, The circadian clock and human health. *Curr Biol* **26**, R432-43 (2016).
743 9. J.D. Johnston, J.M. Ordovás, F.A. Scheer, F.W. Turek, Circadian rhythms, metabolism, and
744 chrononutrition in rodents and humans. *Adv Nutr* **7**, 399-406 (2016).
745 10. E. N. C. Manoogian, A. Chaix, S. Panda, When to eat: The importance of eating patterns in health
746 and disease. *J Biol Rhythms* **34**, 579–581 (2019).
747 11. L. R. Wegrzyn, *et al.*, Rotating night-shift work and the risk of breast cancer in the Nurses' Health
748 Studies. *Am J Epidemiol* **186**, 532–540 (2017).
749 12. A.M. Ramsey, A. Stowie, O. Castanon-Cervantes, A.J. Davidson, Environmental circadian
750 disruption increases stroke severity and dysregulates immune response. *J Biol Rhythms* **35**, 368-376
751 (2020).
752 13. W.H. Walker,2nd, J. C. Walton, A. C. DeVries, R. J. Nelson, Circadian rhythm disruption and
753 mental health. *Transl Psychiatry* **10**, 28 (2020).
754 14. T. Papagiannakopoulos, *et al.*, Circadian rhythm disruption promotes lung tumorigenesis. *Cell*
755 *Metab* **24**, 324–331 (2016).
756 15. E. Hadadi, *et al.*, Chronic circadian disruption modulates breast cancer stemness and immune
757 microenvironment to drive metastasis in mice. *Nat Commun* **11**, 3193-020-16890–6 (2020).

758 16. A. J. Millar, S. R. Short, N. H. Chua, S. A. Kay, A novel circadian phenotype based on firefly
759 luciferase expression in transgenic plants. *Plant Cell* **4**, 1075–1087 (1992).
760 17. T. Kondo, *et al.*, Circadian rhythms in prokaryotes: luciferase as a reporter of circadian gene
761 expression in cyanobacteria. *Proc Natl Acad Sci U S A* **90**, 5672–5676 (1993).
762 18. C. Brandes*, et al.,* Novel features of *Drosophila period* transcription revealed by real-time luciferase
763 reporting*. Neuron* **16,** 687-692 (1996).
764 19. D.K. Welsh, S.H. Yoo, A.C. Liu, J.S. Takahashi, S.A. Kay, Bioluminescence imaging of individual
765 fibroblasts reveals persistent, independently phased circadian rhythms of clock gene expression.
766 *Curr Biol* **14**, 2289-2295 (2004).
767 20. E. Nagoshi, *et al.*, Circadian gene expression in individual fibroblasts: cell-autonomous and self-
768 sustained oscillators pass time to daughter cells. *Cell* **119**, 693–705 (2004).
769 21. S. Yamazaki, *et al.*, Resetting central and peripheral circadian oscillators in transgenic rats. *Science*
770 **288**, 682–685 (2000).
771 22. M. Abe, *et al.*, Circadian rhythms in isolated brain regions. *J Neurosci* **22**, 350–356 (2002).
772 23. S. H. Yoo, *et al.*, PERIOD2::LUCIFERASE real-time reporting of circadian dynamics reveals
773 persistent circadian oscillations in mouse peripheral tissues. *Proc Natl Acad Sci U S A* **101**, 5339–
774 5346 (2004).
775 24. R. Stanewsky, *et al.*, The *cry*^{b} mutation identifies cryptochrome as a circadian photoreceptor in
776 *Drosophila*. *Cell* **95**, 681–692 (1998).
777 25. E. E. Zhang, *et al.,* A genome-wide RNAi screen for modulators of the circadian clock in human
778 cells. *Cell* **139**, 199-210 (2009).
779 26. T. Hirota T, *et al.,* High-throughput chemical screen identified a novel potent modulator of cellular
780 circadian rhythms and reveals CK1 as a clock regulatory kinase. *PLoS Biol* **8**, e1000559 (2010).
781 https://doi.org/10.1371/journal.pbio.1000559.
782 27. T. Hirota T, *et al.,* Identification of small molecule activators of cryptochrome. *Science* **337**, 1094-
783 1097 (2012).
784 28. Z. Chen, *et al.*, Identification of diverse modulators of central and peripheral circadian clocks by
785 high-throughput chemical screening. *Proc Natl Acad Sci U S A* **109**, 101–106 (2012).
786 29. W. Nakamura, S. Yamazaki , N.N. Takasu, K. Mishima, G.D. Block GD, Differential response of
787 *period 1* expression within the suprachiasmatic nucleus*. J Neurosci* **25**, 5481-5487 (2005).
788 30. Y. Yamanaka, S. Honma, K-I Honma, Scheduled exposures to a novel environment with a running-
789 wheel differentially accelerate re-entrainment of mice peripheral clocks to new light-dark cycles*.*
790 *Genes Cells* **13**, 497-507(2008).

791 31. A. J. Davidson, S. Yamazaki, D. M. Arble, M. Menaker, G. D. Block, Resetting of central and
792 peripheral circadian oscillators in aged rats. *Neurobiol Aging* **29**, 471–477 (2008).
793 32. A. J. Davidson, O. Castanon-Cervantes, T. L. Leise, P. C. Molyneux, M. E. Harrington, Visualizing
794 jet lag in the mouse suprachiasmatic nucleus and peripheral circadian timing system. *Eur J*
795 *Neurosci* **29**, 171–180 (2009).
796 33. M. T. Sellix, *et al.*, Aging differentially affects the re-entrainment response of central and peripheral
797 circadian oscillators. *J Neurosci* **32**, 16193–16202 (2012).
798 34. P. Pezuk, J. A. Mohawk, L. A. Wang, M. Menaker, Glucocorticoids as entraining signals for
799 peripheral circadian oscillators. *Endocrinology* **153**, 4775–4783 (2012).
800 35. K. A. Stokkan, S. Yamazaki, H. Tei, Y. Sakaki, M. Menaker, Entrainment of the circadian clock in
801 the liver by feeding. *Science* **291**, 490–493 (2001).
802 36. A. Balsalobre, *et al.*, Resetting of circadian time in peripheral tissues by glucocorticoid
803 signaling. **289**, 2344–2347 (2000).
804 37. A. Balsalobre, F. Damiola, U. Schibler, A serum shock induces circadian gene expression in
805 mammalian tissue culture cells. *Cell* 93(6): 929-937(1998).
806 38. F. Damiola, *et al.*, Restricted feeding uncouples circadian oscillators in peripheral tissues from the
807 central pacemaker in the suprachiasmatic nucleus. *Genes Dev* **14**, 2950–2961 (2000).
808 39. A. B. Reddy, M. D. Field, E. S. Maywood, M. H. Hastings, Differential resynchronisation of
809 circadian clock gene expression within the suprachiasmatic nuclei of mice subjected to experimental
810 jet lag. *J Neurosci* **22**, 7326–7330 (2002).
811 40. M. Nagano, *et al.*, An abrupt shift in the day/night cycle causes desynchrony in the mammalian
812 circadian center. *J Neurosci* **23**, 6141–6151 (2003).
813 41. Y. Yamaguchi, *et al.*, Mice genetically deficient in vasopressin V1a and V1b receptors are resistant
814 to jet lag. *Science* **342**, 85-90 (2013).
815 42. E. Destici, E.H. Jacobs, F. Tamanini, M. Loos, G.T.J. van der Horst, M. Oklejewicz, Altered phase-
816 relationship between peripheral oscillators and environmental time in *Cry1* or *Cry2* deficient mouse
817 models for early and late chronotypes. *PLoS ONE* ***8, e83802 (2013).***
818 43. S. K. Nicholls, L. P. Casiraghi, W. Wang, E. T. Weber, M. E. Harrington, Evidence for internal
819 desynchrony caused by circadian clock resetting. *Yale J Biol Med* **92**, 259–270 (2019).
820 44. W. Nakamura, *et al.*, *In vivo* monitoring of circadian timing in freely moving mice. **18**, 381–385
821 (2008).
822 45. D. Ono, K. Honma, S. Honma, Circadian and ultradian rhythms of clock gene expression in the
823 suprachiasmatic nucleus of freely moving mice. *Sci Rep* **5**, 12310 (2015).

824 46. D. Ono, S. Honma, K. Honma, Circadian PER2::LUC rhythms in the olfactory bulb of freely
825 moving mice depend on the suprachiasmatic nucleus but not on behaviour rhythms. *Eur J*
826 *Neurosci* **42**, 3128–3137 (2015).
827 47. D. Ono, *et al.*, Dissociation of *Per1* and *Bmal1* circadian rhythms in the suprachiasmatic nucleus in
828 parallel with behavioral outputs. *Proc Natl Acad Sci U S A* **114**, E3699–E3708 (2017).
829 48. Y. Yamaguchi, *et al*., Real-time recording of circadian *Per1* and *Per2* expression in the
830 suprachiasmatic nucleus of freely moving rats. *J Biol Rhythms* **31**,108-111 (2016).
831 49. L. Mei, *et al.*, Long-term in vivo recording of circadian rhythms in brains of freely moving
832 mice. *Proc Natl Acad Sci U S A* **115**, 4276–4281 (2018).
833 50. T. Hamada, *et al.*, *In vivo* imaging of clock gene expression in multiple tissues of freely moving
834 mice. *Nat Commun* **7**, 11705 (2016).
835 51. Y. Tahara, *et al.*, *In vivo* monitoring of peripheral circadian clocks in the mouse. *Curr Biol* **22**, 1029–
836 1034 (2012).
837 52. V. van der Vinne, B. Martin Burgos, M. E. Harrington, D. R. Weaver, Deconstructing circadian
838 disruption: Assessing the contribution of reduced peripheral oscillator amplitude on obesity and
839 glucose intolerance in mice. *J Pineal Res* e12654 (2020). https://doi.org/10.1111/jpi.12654
840 53. V. van der Vinne, S. J. Swoap, T. J. Vajtay, D. R. Weaver, Desynchrony between brain and
841 peripheral clocks caused by CK1δ/ε disruption in GABA neurons does not lead to adverse metabolic
842 outcomes. *Proc Natl Acad Sci U S A* **115**, E2437–E2446 (2018).
843 54. C. Saini, *et al.*, Real-time recording of circadian liver gene expression in freely moving mice reveals
844 the phase-setting behavior of hepatocyte clocks. *Genes Dev* **27**, 1526–1536 (2013).
845 55. B. Martin-Burgos, W. Wang, I. William, S. Tir, I. Mohammad, R. Javed, S. Smith, Y. Cui, C.B.
846 Smith, V. van der Vinne, P.C. Molyneux, S.C. Miller, D. R. Weaver, T.L. Leise, M.E. Harrington,
847 Methods for detecting PER2::LUCIFERASE bioluminescence rhythms in freely moving mice.
848 BioRxiv 2020 https://doi.org/10.1038/s41467-017-00462-2
849 56. J.H. Kim, *et al*., High cleavage efficiency of a 2A peptide derived from porcine Teschovirus-1 in
850 human cell lines, zebrafish and mice. PLoS ONE **6**, e18556 (2011).
851 doi:10.1371/journal.pone.0018556
852 57. P. Fonjallaz, V. Ossipow, G. Wanner and U. Schibler, The two PAR leucine zipper proteins,
853 TEF and DBP, display similar circadian and tissue-specific expression, but have different
854 target promoter preferences. *EMBO J* **15**, 351-362 (1996).
855 58. E.D. Herzog, T. Hermanstyne, N.J. Smyllie, M.H. Hastings, Regulating the suprachiasmatic nucleus
856 (SCN) Clockwork: Interplay between cell-autonomous and circuit-level mechanisms. *Cold Spring*
857 *Harb Perspect Bio*l **9**, a027706 (2017).

858 59. I. T. Lee, *et al.*, Neuromedin S-producing neurons act as essential pacemakers in the suprachiasmatic
859 nucleus to couple clock neurons and dictate circadian rhythms. *Neuron* **85**, 1086–1102 (2015).
860 60. Y. Shan, *et al.*, Dual-color single-cell imaging of the suprachiasmatic nucleus reveals a circadian
861 role in network synchrony. *Neuron* **108**, 164-179 (2020).
862 61. M. Mieda, *et al.*, Cellular clocks in AVP neurons of the SCN are critical for interneuronal coupling
863 regulating circadian behavior rhythm. *Curr Biol* **85**, 1103–1116 (2015).
864 62. M. Mieda, H. Okamoto, T. Sakurai, Manipulating the cellular circadian period of arginine
865 vasopressin neurons alters the behavioral circadian period. *Neuron* **26**, 2535–2542 (2016).
866 63. N. J. Smyllie, J. E. Chesham, R. Hamnett, E. S. Maywood, M. H. Hastings, Temporally chimeric
867 mice reveal flexibility of circadian period-setting in the suprachiasmatic nucleus. *Proc Natl Acad Sci*
868 *U S A* **113**, 3657–3662 (2016).
869 64. M. Brancaccio, *et al.*, Cell-autonomous clock of astrocytes drives circadian behavior in
870 mammals. *Science* **363**, 187–192 (2019).
871 65. R.C. Poulsen, *et al.,* How does general anaesthesia affect the circadian clock? *Sleep Med Rev.* **37**,
872 35-44 (2018).
873 66. Y. Sawai, *et al*., *In vivo* evaluation of the effect of lithium on peripheral circadian clocks by real-
874 time monitoring of clock gene expression in near-freely moving mice. *Sci Comm* **9**, 10909 (2019).
875 67. K. Hamada K, *et al*., Double recording system of *Period1* gene expression rhythm in the olfactory
876 bulb and liver of freely moving mouse. *Biochem Biophys Res Comm* **529**, 898-903 (2020).
877 68. S. Yamaguchi, *et al.*, View of a mouse clock gene ticking. *Nature* **409**, 684 (2001).
878 69. Acosta-Rodriguez, M.H.M. de Groot, F. Rijo-Ferreira, C.B. Green, J. S. Takahashi, Mice under
879 caloric restriction self-impose a temporal restriction of food intake as revealed by an automated
880 feeder system. *Cell Metab* **26**, 267-277 (2017).
881 70. T. Noguchi, *et al.*, Circadian rhythm bifurcation induces flexible phase resetting by reducing
882 circadian amplitude. *Eur J Neurosci* **51**, 2329–2342 (2020).
883 71. T. L. Leise, *et al.*, Recurring circadian disruption alters circadian clock sensitivity to resetting. *Eur J*
884 *Neurosci* **51**, 2343–2354 (2020).
885 72. L. Lopez-Molina *et al.*, The DBP gene is expressed according to a circadian rhythm in the
886 suprachiasmatic nucleus and influences circadian behavior. *EMBO J* **16**, 6762-6771 (1997).
887 73. M.S. Evans, *et al*., A synthetic luciferin improves bioluminescence imaging in live mice. *Nat*
888 *Methods* **11**, 393-395 (2014).
889 74. S. Iwano, *et al*., Single-cell bioluminescence imaging of deep tissue in freely moving animals.
890 *Science* **359**, 935-939 (2018).

891 75. J.E. Miller, *et al*., Vasoactive intestinal polypeptide mediates circadian rhythms in mammalian
892 olfactory bulb and olfaction. *J Neurosci* **34**, 6040-6046 (2014).
893 76. X. Xie, et al., Natural food intake patterns have little synchronizing effect on peripheral circadian
894 clocks. *BMC Biology* ***18***, 160 (2020). https://doi.org/10.1186/s12915-020-00872-7
895 77. F. Sinturel, *et al*., Circadian hepatocyte clocks keep synchrony in the absence of a master pacemaker
896 in the suprachiasmatic nucleus or other extrahepatic clocks. *Genes Dev* **35,** (e-pub ahead of print)
897 (2021). http://www.genesdev.org/cgi/doi/10.1101/gad.346460.120
898 78. S. H. Yoo, *et al.*, *Period2* 3′-UTR and microRNA-24 regulate circadian rhythms by repressing
899 PERIOD2 protein accumulation. *Proc Natl Acad Sci U S A* **114**, E8855–E8864 (2017).
900 79. D. R. Weaver, *et al.*, Functionally complete excision of conditional alleles in the mouse
901 suprachiasmatic nucleus by *Vgat-ires-Cre*. *J Biol Rhythms* **33**, 179–191 (2018).
902 80. S. Yamazaki, J. S. Takahashi, Real-time luminescence reporting of circadian gene expression in
903 mammals. *Methods* **393**, 288–301 (2005).
904 81. J. A. Evans, T. L. Leise, O. Castanon-Cervantes, A. J. Davidson, Intrinsic regulation of
905 spatiotemporal organization within the suprachiasmatic nucleus. *PLoS ONE* **6**, e15869 (2011).
906 82. J. A. Evans, T. L. Leise, O. Castanon-Cervantes, A. J. Davidson, Dynamic interactions mediated by
907 nonredundant signaling mechanisms couple circadian clock neurons. *Neuron* **80**, 973–983 (2013).
908 83. T. L. Leise, M. E. Harrington, Wavelet-based time series analysis of circadian rhythms. *J Biol*
909 *Rhythms* **26**, 454–463 (2011).
910 84. T. L. Leise, Analysis of nonstationary time series for biological rhythms research. *J Biol Rhythms*
911 **32**, 187–194 (2017).
912 85. T. L. Leise, *et al.*, Voluntary exercise can strengthen the circadian system in aged mice. *Age (Dordr)*
913 **35**, 2137–2152 (2013).

914 **Figures and Tables**

915

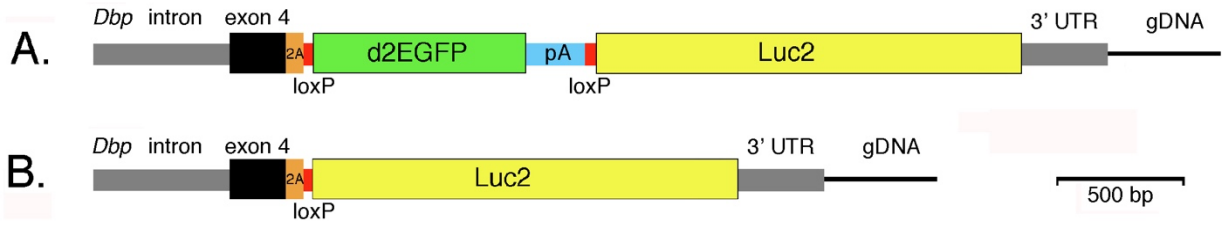

916

917 **Figure 1. Generation of a bifunctional reporter from the mouse *Dbp* locus.**

918 **A.** The mouse *Dbp* locus was modified by CRISPR-mediated insertion of the donor construct shown. The
919 construct contained homology arms from the *Dbp* locus (gray and black) and inserted the reporter sequences
920 with a T2A-encoding sequence (orange) between DBP and the reporter. Destabilized EGFP (d2EGFP) with
921 a bovine growth hormone polyadenylation site (PA) was flanked by *loxP* sites (red). Downstream of *GFP*
922 is a luciferase (*Luc2*) reporter gene. Without recombination *Dbp* and *GFP* are expressed as a single
923 transcript from the conditional (Dbp^{KI} allele).

924 **B.** With *Cre*-mediated recombination, GFP-encoding sequences are excised and *Dbp* and *luciferase* are
925 expressed as a single transcript. The T2A sequence generates separate proteins from these bifunctional
926 transcripts. *Cre*-mediated germline recombination led to mice expressing luciferase non-conditionally from
927 the Dbp^{Luc} allele.

928

929 *File: Fig 1 Construct figure copy_drw121120.jpg*

930

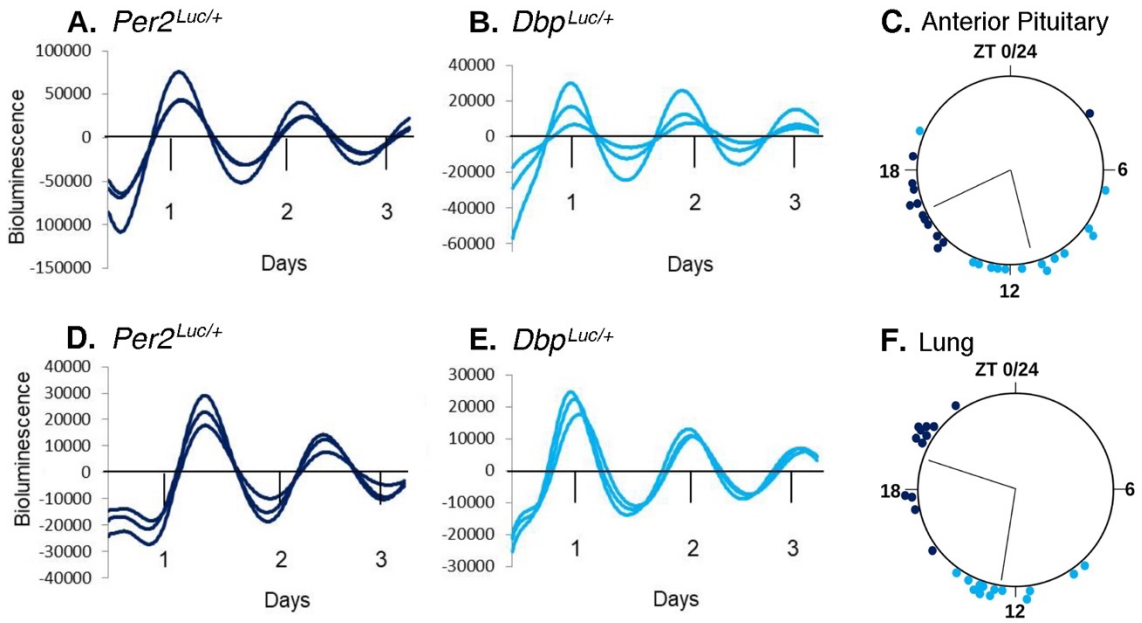

931

932

933 **Figure 2. Tissue explants from *Dbp*$^{Luc/+}$ mice have an earlier time of peak bioluminescence than**
934 **explants from *Per2*$^{Luc/+}$ mice *in vitro.***

935 **A-C**, Anterior Pituitary gland explants. **D-F**, Lung explants.

936 **A., B., D., and E**. are representative bioluminescence rhythms from triplicate tissue explants from *Per2*$^{Luc/+}$
937 (**A, D**) and *Dbp*$^{Luc/+}$ mice (**B, E**). 'Days' refers to time in culture, not projected ZT. Values are 24-h
938 background-subtracted, 3-h smoothed values.

939 **C,F.** Time of peak bioluminescence *in vitro.* The large circles represent a 24-h day for each organ. ZT's
940 refer to the lighting cycle to which the mice were exposed prior to sample collection, with ZT0-12 being
941 the light phase. Colored points at the perimeter of the large circle indicate the timing of peak
942 bioluminescence of individual *Per2*$^{Luc/+}$ (dark blue) or *Dbp*$^{Luc/+}$ (teal) tissue explants (n=12-14 mice).
943 Within each tissue/genotype combination, there was significant clustering of times of peak
944 bioluminescence. Radial lines represent the mean peak time, which differed significantly between
945 genotypes for each tissue (Watson-Williams test, $p<0.001$).

946

947 *File: Fig 2 in vitro-032821.jpg*

948

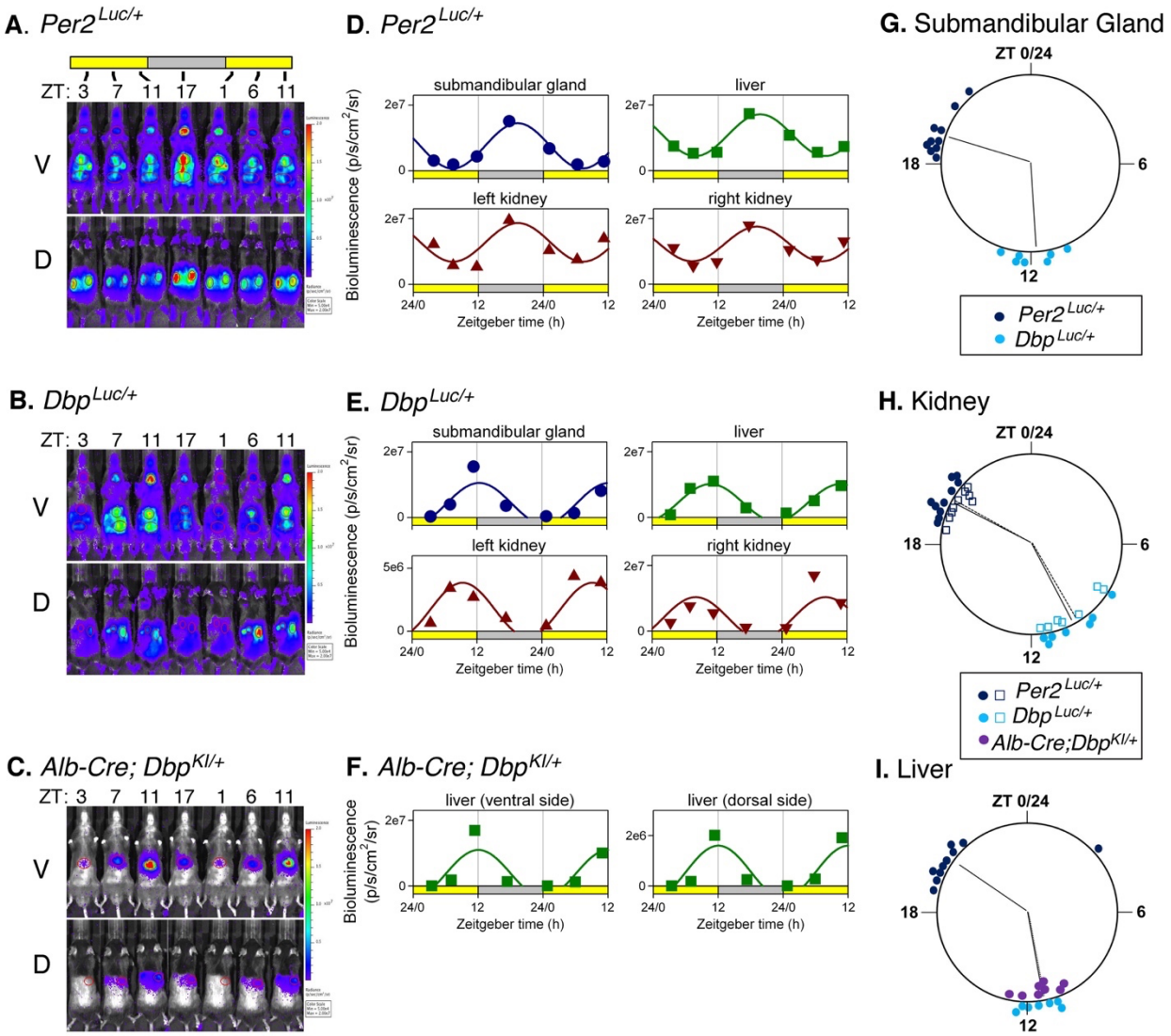

Figure 3. Bioluminescence rhythms measured *in vivo*

A-C. Bioluminescence images captured at 4-6 hr intervals from a representative mouse of each genotype. **A**. *Per2*$^{Luc/+}$, **B**. *Dbp*$^{Luc/+}$ **C**. *Alb-Cre+ ; Dbp*$^{KI/+}$. Ventral (V) and dorsal (D) views are shown for each mouse. All images for each mouse are set to the same luminescence scale.

D-F. Cosinor-fitting of bioluminescence signal over time for the animals shown in Panels A-C to determine peak time. Bioluminescence rhythms were assessed in submandibular gland, liver, and kidneys of (**D.**) *Per2*$^{Luc/+}$ and (**E.**) *Dbp*$^{Luc/+}$ reporter mice, and from liver of *Alb-Cre+ ; Dbp*$^{KI/+}$ mice (**F.**).

G-I. Time of peak bioluminescence *in vivo* as assessed by IVIS imaging. **G.** Submandibular gland, **H.** Kidneys, and **I.** Liver. Data plotted as in Fig. 2C and 2F. Dark blue symbols are *Per2*$^{Luc/+}$ tissues (n=10), teal symbols are *Dbp*$^{Luc/+}$ tissues (n=7). In Panel H, open symbols represent the right kidney and filled symbols represent the left kidney. In Panel I, purple circles represent livers from *Alb-Cre+ ; Dbp*$^{KI/+}$ mice

961 (n=8). Radial lines represent the mean peak time for each genotype and tissue. Radial lines from the two
962 kidneys of a genotype are nearly overlapping. For liver, radial lines for the two *Dbp* reporter lines are
963 overlapping and appear as a single line. Time of peak for each $Per2^{Luc/+}$ organ examined differed
964 significantly from time of peak of the corresponding organs from $Dbp^{Luc/+}$ and *Alb-Cre+ ;* $Dbp^{KI/+}$ mice
965 (p=0.002, Watson-Williams test). There was no significant difference in peak time between *DbpLuc/+* and
966 *Alb-Cre+ ;* $Dbp^{KI/+}$ liver tissues (P >0.05).
967
968 *File: Fig 3 in vivo IVIS_032821scaled.jpg*

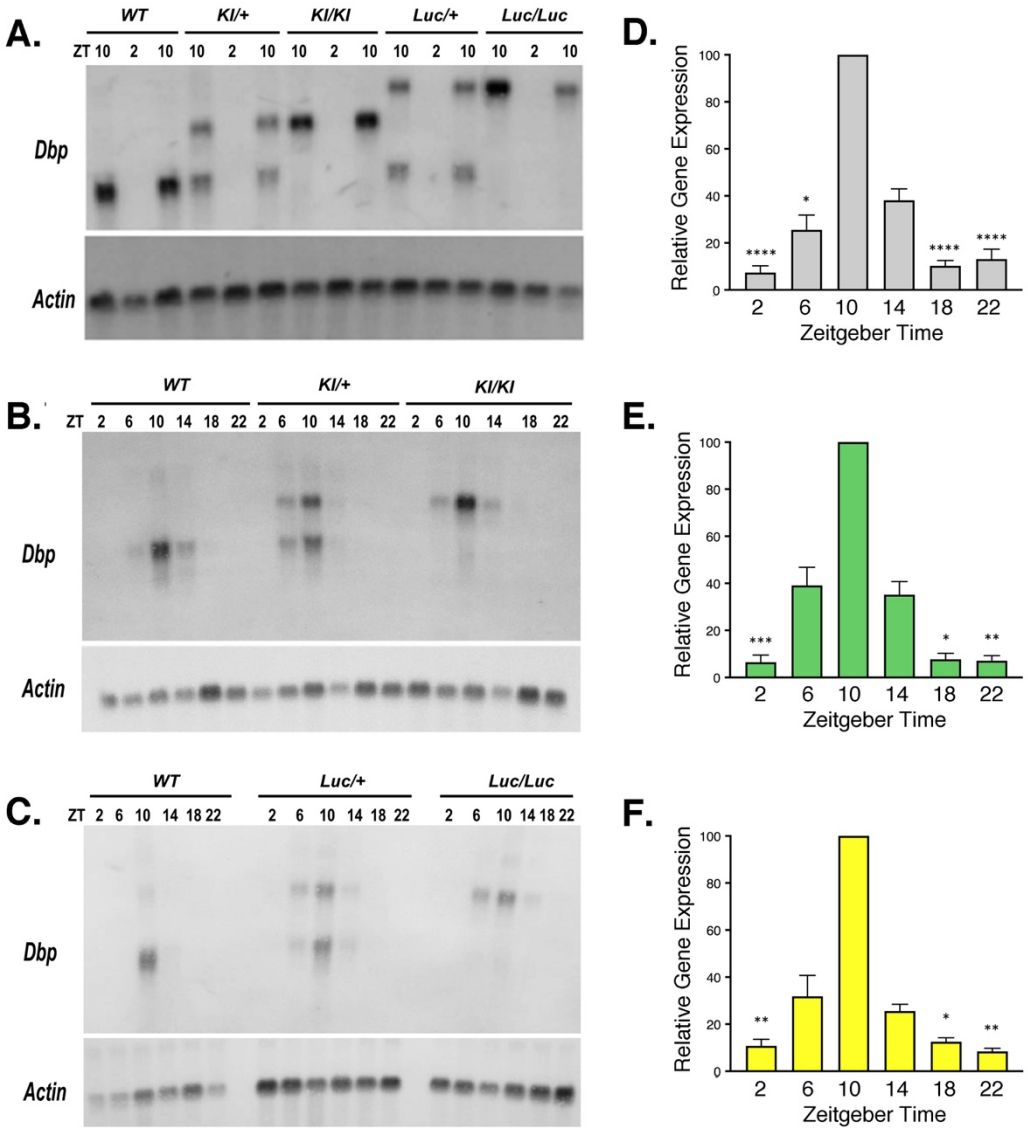

Figure 4. *Dbp* mRNA rhythms are not altered in reporter mice

A-C. Representative Northern Blots probed to detect *Dbp* and *Actin* mRNA. **A.** From each of five genotypes, RNA samples were extracted from livers collected at ZT 2 and 10. For each genotype, there are two samples at ZT10 and one sample at ZT2 on this blot. **B**. and **C**. Representative Northern Blots of RNA samples collected from WT and reporter mouse livers at each of six Zeitgeber times (ZT).

D-F. Quantification of *Dbp* mRNA rhythms for each allele in time-series experiments (6 time-points each). Results are expressed as mean (± SEM) percent of the peak *Dbp*/Actin ratio, which occurred at ZT 10 on every blot. **D.** Wild-type *Dbp* transcript (n=12 sample sets). **E.** Dbp^{KI} transcript (n= 6). **F.** Dbp^{Luc} transcript (n= 6). For each transcript, there was a significant rhythm (Friedman's One-way ANOVA, Q > 19, $p < 0.002$). Asterisks indicate time-points that differed significantly from ZT10 (Dunn's test, * $p < 0.05$, ** p

980 < 0.01, *** $p < 0.001$, **** $p \leq 0.0001$). Significant differences among some other time-points are not
981 shown for clarity.
982
983 *File: Fig 4_Northern figure with bar graphs_010321.jpg*

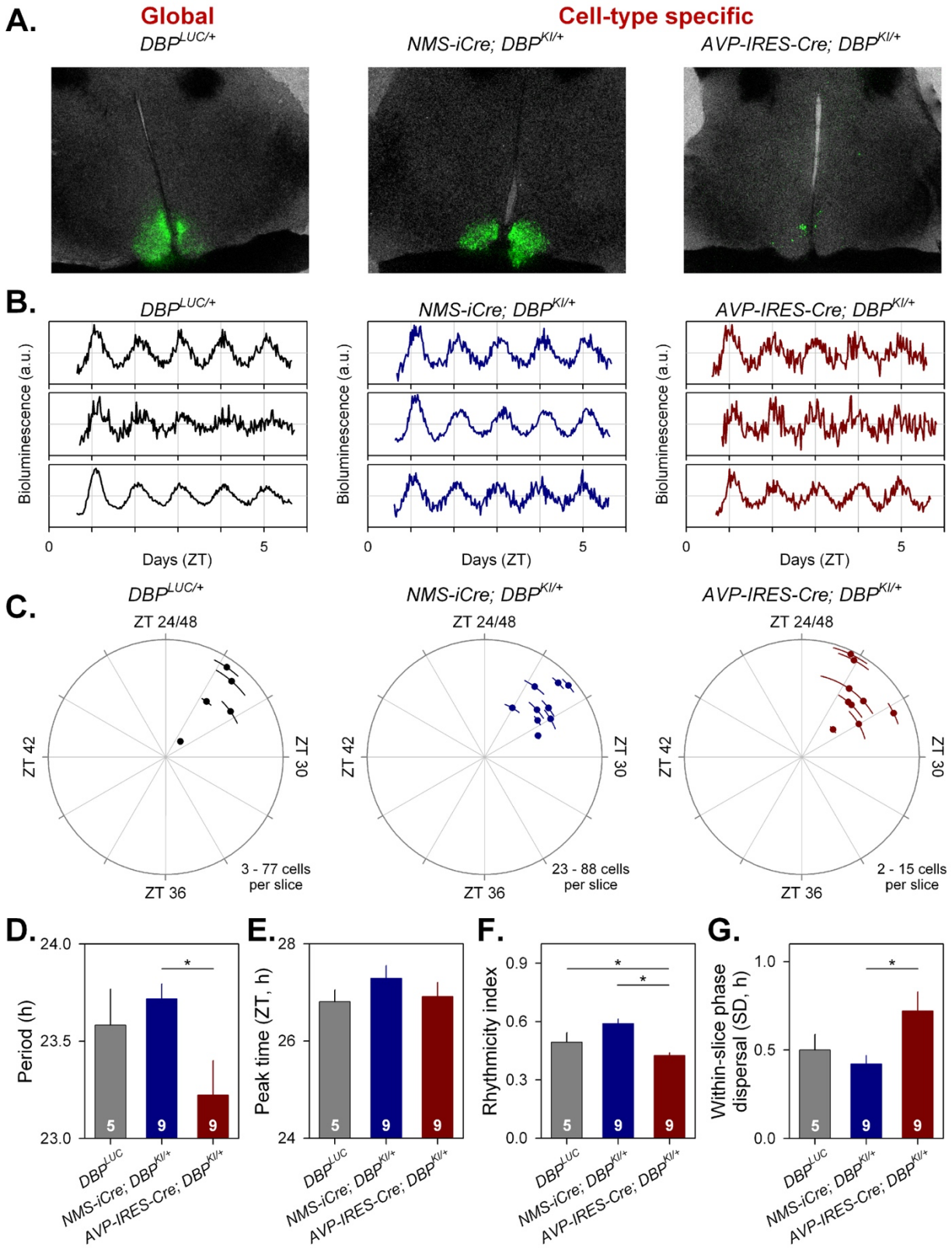

Figure 5. Cell-type-specific imaging of LUCIFERASE expression in SCN slices

987 **A)** 24h summed bioluminescence overlaid onto bright field images of a section through the SCN from
988 *DBP*$^{Luc/+}$ (global reporter expression, left), and in mice expressing luciferase from specific subsets of SCN
989 neurons (NMS^{+} cells, center; AVP^{+} cells, right).
990 **B.** Representative bioluminescence traces from single neuron-like ROIs in slices from each genotype.
991 **C.** Circular plots indicate the peak time of bioluminescence rhythms from each genotype. Time is expressed
992 relative to the light-dark cycle the mice were housed in prior to sacrifice; numbers >24 are used to indicate
993 that these measures are recorded on the first day *in vitro* and are plotted relative to previous *in vivo* lighting
994 conditions. Each slice is represented by a small dot. Placement of the dot relative to outer circle indicates
995 average peak time (±SD), while the distance from the center corresponds to the number of cells incorporated
996 in the average (√cell#).
997 **D.** Mean period (± SEM) by genotype. The number of slices per genotype is indicated at the base of each
998 bar (D-G).
999 **E**. Circular mean peak time (± SEM) by genotype.
1000 **F.** Mean rhythmicity index score (± SEM) by genotype.
1001 **G.** Mean peak time dispersal (quantified by circular SD of peak times within each slice) by genotype.
1002
1003 *File: Fig 5_Smith et al_032821.jpg*

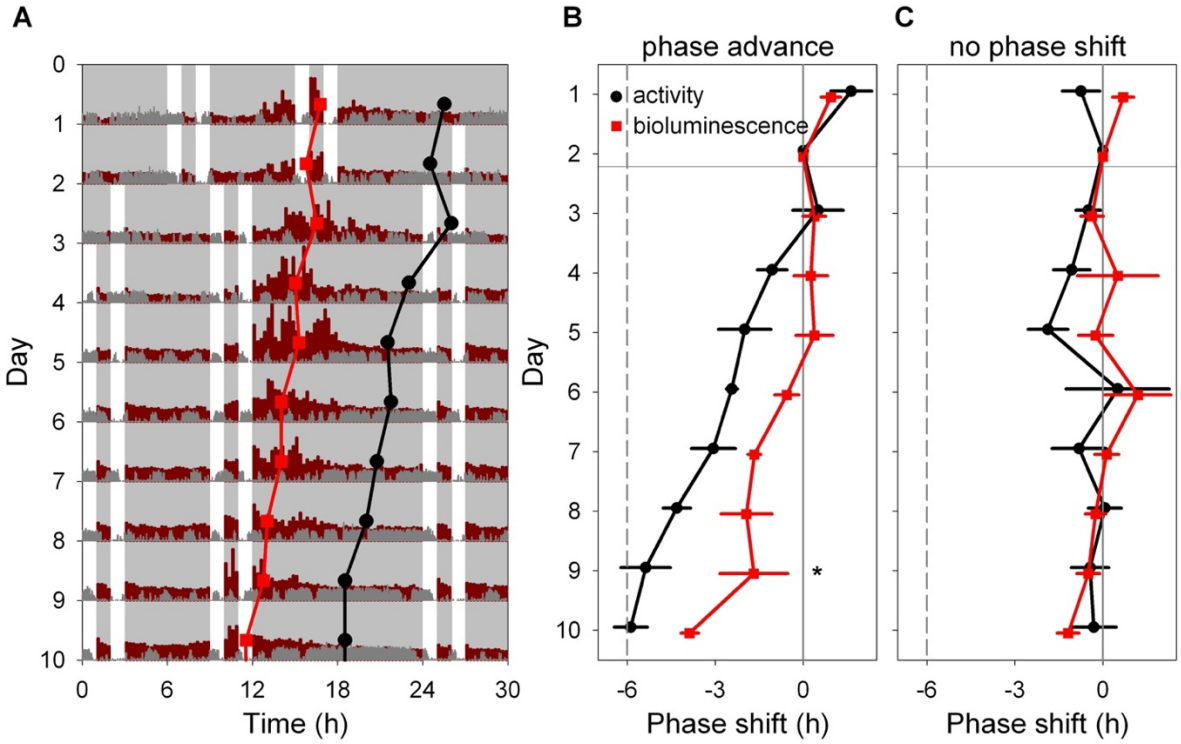

Figure 6. Light-induced resetting produces misalignment between liver bioluminescence rhythms and locomotor activity rhythms.

A. Representative double-plotted actogram showing locomotor activity (dark gray) and bioluminescence (dark red) of an *Alb-Cre; Dbp*$^{KI/+}$ liver reporter mouse before and after a 6-h advance of the skeleton photoperiod consisting of four 1-h periods of light per 24-h day, as indicated by white. The skeleton photoperiod was advanced by 6 h by shortening the dark phase after the last light pulse on Day 2. Red squares represent the peak of the bioluminescence rhythm, while black circles represent the midpoint of locomotor activity each day. These values were determined by discrete wavelet transform analysis. Six hours of each cycle are double-plotted to aid visualization of the data. Light and dark are indicated by white and light-gray backgrounds, respectively.

B. Mean (± SEM) midpoint of locomotor activity (black) and peak of liver bioluminescence (red) rhythms are shown, relative to their initial value, in a group of 4 mice exposed to a shifted skeleton photoperiod. Both rhythms reset gradually after a 6-h phase advance of the skeleton photoperiod, but the locomotor activity rhythm re-sets more rapidly than the bioluminescence rhythm within animal (Significant Measure * Day interaction, and significant phase difference between the rhythms on Day 9 (Tukey HSD, p <0 .05).

C. Mean (± SEM) time of midpoint of locomotor activity (black) and peak liver bioluminescence (red) rhythms are shown, relative to their initial phase, in a group of 4 mice not subjected to a phase shift of the skeleton photoperiod.

1023
1024 *File: Fig 6_Liver Reporter SPP phase shift.JPG*
1025

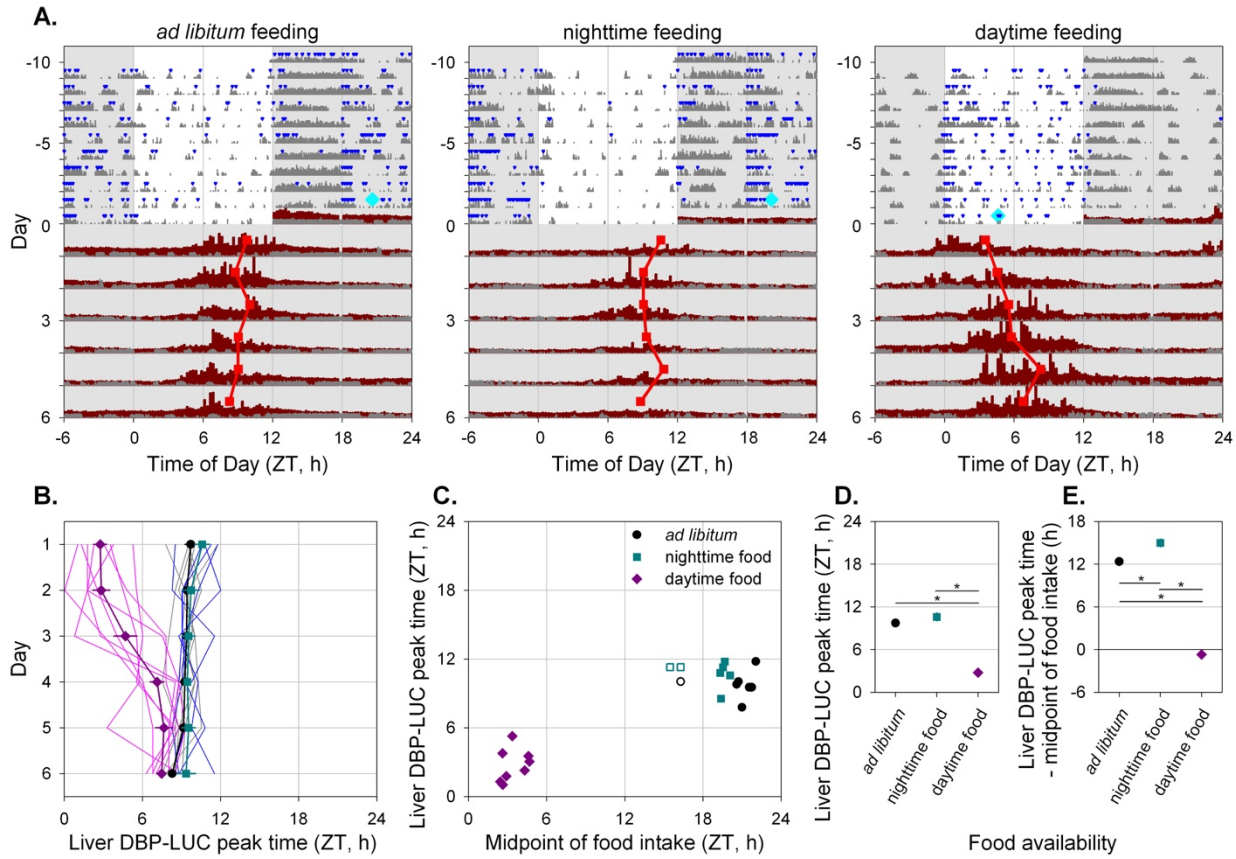

Figure 7. Time-restricted feeding alters the timing of liver bioluminescence rhythms.

A. Representative actograms of three *Alb-Cre; Dbp*$^{KI/+}$ liver reporter mice exposed to the different feeding regimes as indicated above each panel. Mice were housed in a 12h:12h light-dark cycle and exposed to the specified feeding regime for ten days (-10 to 0) preceding bioluminescence recording. The timing of food intake (blue triangles) and general locomotor activity (dark gray) was recorded continuously. The midpoint of food intake over the last five days preceding bioluminescence recording is indicated by a cyan diamond on day 0. Mice were transferred to the bioluminescence recording setup at the start of the dark phase and housed in constant darkness with *ad libitum* food access starting 12 hr later. Liver bioluminescence levels are depicted in dark red. Red squares represent the time of peak of the bioluminescence rhythm, determined by discrete wavelet transform. Six hours of each cycle are double-plotted and the y-axis has been stretched during the last 6 days to aid visualization of the data. Light and dark are indicated by white and light gray backgrounds, respectively.

B. Individual and mean (± SEM) phase of liver bioluminescence rhythms relative to clock time for three feeding groups. Mice previously exposed to *ad libitum*, nighttime and daytime feeding are plotted in grey/black, blue/cyan and magenta, respectively (key in Panel C). Prior to recording

1043 bioluminescence, mice were entrained to a 12L:12D lighting cycle with lights on at 0600. Mice
1044 previously exposed to daytime feeding show an advanced peak phase of liver bioluminescence that
1045 reverts over time in constant darkness with *ad libitum* food.

1046 **C.** Relationship between preceding feeding phase and peak liver bioluminescence phase for individual
1047 animals on the first day under constant conditions. *Ad libitum* and night-fed groups had similar
1048 midpoint of food intake; three "outliers" with respect to midpoint of food intake (shown by open
1049 symbols) were not included in further analyses (Panels B, D and E).

1050 **D.** Mean (± SEM) peak liver bioluminescence phase on the first day under constant conditions, relative
1051 to clock time for the three feeding regimens. The low variability within groups resulted in error bars
1052 that were nearly or completely contained within the symbols.

1053 **E.** Mean (±SEM) peak liver bioluminescence phase on the first day under constant conditions, relative
1054 to the midpoint of preceding food intake for the three feeding regimens. The low variability within
1055 groups resulted in error bars that were nearly or completely contained within the symbols.

1056

1057 *File: Fig 7_Smith et al_032921.JPG*

1058

1059 **Table 1:** Period length of locomotor activity rhythms in constant darkness, by sex and genotype

1060

Genotype	Sex	N	tau_{DD} (Mean +/- SEM), h
1061			
1062 *Dbp*$^{+/+}$	Male	15	23.88 ± 0.027
1063 *Dbp*$^{KI/+}$	Male	10	23.91 ± 0.057
1064 *Dbp*$^{KI/KI}$	Male	11	23.92 ± 0.036
1065 *Dbp*$^{Luc/+}$	Male	11	23.86 ± 0.025
1066 *Dbp*$^{Luc/Luc}$	Male	8	23.97 ± 0.029
1067			
1068 *Dbp*$^{+/+}$	Female	21	23.87 ± 0.021
1069 *Dbp*$^{KI/+}$	Female	9	23.89 ± 0.036
1070 *Dbp*$^{KI/KI}$	Female	11	23.79 ± 0.030
1071 *Dbp*$^{Luc/+}$	Female	8	23.82 ± 0.053
1072 *Dbp*$^{Luc/Luc}$	Female	8	23.75 ± 0.042